Dynamic Characteristics of Regional Flows around the Pyrénées in View of the PYREX Experiment. Part I: Analysis of the Pressure and Wind Fields and Experimental Assessment of the Applicability of the Linear Theory

B. BÉNECH, E. KOFFI, A. DRUILHET, AND P. DURAND

Laboratoire d'Aerologie, Universite Paul Sabatier, Toulouse, France

P. BESSEMOULIN

Centre National de Recherches Meteorologiques, Meteo-France, Toulouse, France

J. CAMPINS AND A. JANSA

Centro Meteorologico de Baleares, Instituto Nacional de Meteorologia, Palma de Mallorca, Spain

B. TERLIUC

Department of Environmental Researches, Nuclear Research Centre, Negev, Israel

(Manuscript received 29 July 1996, in final form 25 April 1997)

ABSTRACT

The Pyrénées experiment (PYREX), launched by the French and Spanish meteorological services, had provided an extensive database that was used in the present work to describe the airflow around the Pyrénées and to evaluate the applicability of the linear theory to stable flows that are blocked by a relatively large mountain range.

The direction of incidence of the incoming synoptic wind was used to classify the flow in northerly and southerly categories. In both categories, the directions of incidence bear westward from normal incidence to the main axis of the mountain range. Froude (Fr) and Rossby (Ro) numbers were used to represent the thermodynamic characteristics of the incoming air masses and the scale of interaction in terms of the mountain shape. Here, Fr and Ro were found linearly correlated, and their combination corresponding to blocked flow in all the cases.

Average cross correlations between the pressure drag across the mountain and the vertical profiles of the wind components at selected locations demonstrate that the horizontal flow is clearly separated in an upper undisturbed regime and a lower blocked regime in which regional winds are induced. The separating layer corresponding to the mean Froude number encountered during PYREX was found at an altitude of about two-thirds of the mountaintop. Due to the perturbation induced by the deflected wind, the total wind during northerly flows is stronger on the east side than on the west side, while during southerly incoming flows, the total wind distribution is almost symmetric.

Good correlation was found among the pressure field perturbation, the pressure drag, and Froude number of the incoming flow. Clear correlation rules can be deduced from the analysis of the experimental data at different altitudes for both categories of incoming flows. Therefore, since the pressure drag can be easily determined using field measurements, it becomes a powerful tool for the prediction of the regional winds around the Pyrénées.

The experimental data are in agreement with the linear theory predictions of the linear model in Koffi et al. regarding (a) the perturbation of the surface pressure field, which resembles the predicted bipolar distribution; (b) the dependence of the drag on Fr^{-1}, which enables the assessment of the linear theory and the definition of the conditions of applicability of two models [(i) a two-dimensional model, for which it was possible to define quantitatively the effective blocked area, and (ii) a three-dimensional model, for which a scaling function that combines the direction of incidence, the mountain shape, and the Coriolis effect was found almost constant, with an average value of 0.2 for all the cases under study]; (c) the extension of the area affected by the blocking effect, estimated to be 4.5–5 times the width of the barrier and the drift of the strong deceleration point due to the Coriolis effect; (d) the dependence of the wind velocities on Fr^{-1} at the edges of the barrier; and (e) the asymmetric flow deviation induced by the Coriolis effect and biased by the departure of the flow from normal incidence.

Corresponding author address: Bruno Benech, Centre de Recheches Atmosphériques, 65300 Lannemezan, France.
E-mail: benb@aero.obs-mip.fr

1. Introduction

During the period 1 October to 30 November 1990, an experimental program named PYREX (Pyrénées experiment) (Bougeault et al. 1990) was conducted in both sides of the French–Spanish border to carry out intensive measurements of the flow in the Pyrénées area. PYREX was directed to the study of the influence of the mountain range on the atmospheric dynamic flow.

The most current dimensionless numbers used in studies concerning airflow around an obstacle to characterize the obstacle geometry, the incoming air mass, and the earth rotation and gravitation effects are (Smith 1989)

$$\gamma = a/b, \tag{1}$$

the aspect ratio of the mountain range, and

$$\mathrm{Fr} = V/NH, \tag{2}$$

the vertical Froude number, where N is the Brunt–Väisälä frequency [defined by Eq. (5) hereafter] and H is the height of the mountain range. The Froude number is a gauge of the buoyancy of the flow and an important factor to be accounted for in the assessment of the nonlinearity of the flow, as is shown hereafter. The Rossby number is

$$\mathrm{Ro} = V/fa \tag{3}$$

where V is the component of the mean wind velocity normal to the obstacle that has a characteristic length a and f is the Coriolis parameter. Here, Ro quantifies the effect of the earth's rotation on the flow deviation near the obstacle.

Numerical simulations performed by Pierrehumbert and Wyman (1985) show that upstream blocking and lateral deviation of the airflow, resulting in the formation of winds in the vicinity of the mountain, occur under either of the following conditions:

$$\mathrm{Fr} \leq 1 \quad \text{and} \quad \mathrm{Ro} \geq 1$$

or

$$\mathrm{Fr/Ro} < 1 \quad \text{and} \quad \mathrm{Ro} < 1. \tag{4}$$

The ratio Fr/Ro can be separated in two fractions (Pierrehumbert 1984): $(f/N)(a/H)$. The ratio (f/N) describes the ''atmospheric dynamic slope'' since N is a measure of the thermal stability, and f is a measure of the horizontal displacement due to the Coriolis effect. The ratio (a/H) characterizes the mountain slope. If $\mathrm{Fr/Ro} < 1$, the flow is strongly decelerated upstream. When $\mathrm{Fr/Ro} \ll 1$, nonlinear phenomena affect the whole flow in the vicinity of the mountain.

Table 1 shows the values of the parameters mentioned above, based on the results of the soundings carried out in all the PYREX experiment intensive operational periods (IOPs). Since for all the cases under study the atmospheric dynamic slope is only about 10% of the mountain slope and one of the criteria stated in Eq. (4) is always fulfilled, the air masses involved in the experimental conditions are considerably stable and the airflow is expected to become blocked and nonlinear in nature.

The airflow around a topographic obstacle has been studied extensively. Among the cases analyzed are the airflow around an island (Smolarkiewicz and Rotuno 1989; Smith and Grubisic 1993), an isolated mountain (Smith 1980, 1988; Philips 1984; Thorsteinsson 1988; Mass and Ferber 1990), and a large mountain range such as the Alps (Vergeiner 1971; Buzzi and Tibaldi 1977; Smith 1982). Several mechanisms involved in the generation of winds around topographic obstacles can be mentioned: the bipolar pressure anomaly due to blocking effect (Riosalido et al. 1986; Jansa 1987; Campins et al. 1995), the katabatic slope winds foehn and bora in the Alps (Smith 1987), the hydraulic jump in the Rhone valley (Pettre 1982), and the Coriolis effect that induces differential deflections of air masses moving around mountains (Queney 1948; Smith 1979a, 1982).

The three-dimensional wave motion of a uniform flow in the far field of an obstacle was studied by Wurtele (1957), using an extension of the linear theory developed by Lyra (1943) and Queney (1948) for a two-dimensional barrier. In a theoretical study, Drazin (1961) showed that highly stable flows are almost completely split by three-dimensional obstacles. Smith (1980) used the linear theory to describe the steady flow of a stratified Bussinesq fluid over an isolated, small amplitude obstacle and, on the basis of cinematic, dynamic, and energy argumentation, he showed that it becomes inaccurate when the Froude number decreases. Smith (1980) also showed that the small perturbation assumption, used to linearize the equations of motion, is no longer rigorously valid in front of the obstacle for Froude numbers smaller than one, as the first stagnation of the flow appears, while in the lee side, nonlinear wake effects are present when the Froude number decreases to two. Smith (1988) elaborated a solution of the linearized equations of motion in isosteric coordinates to avoid the use of the lower boundary condition at $z = 0$, which is questionable for low Froude numbers, and arrived at similar criteria of validity of the small amplitude assumption as Smith (1980), in terms of density surfaces collapse aloft. The principal inaccuracy near the windward hill surface that arises from the linearization is that some of the isosteres intersect it, beside the formation of a stagnation point.

In spite of some conceptual contradictions and inaccuracies that affect the solution of the linearized equations for small Froude numbers, Smith (1982, 1989) and Phillips (1984) have attempted to extrapolate the linear theory toward dynamic systems for which nonlinear effects are expected to be large. More recently, Stein (1992) carried out numerical simulations with the hydrostatic numerical model PERIDOT (Prévision à Echéance Rapprochèe Intègrant des Données Observées et Tèlèdèteetèes) (Imbard et al. 1986; Bougeault et al.

TABLE 1a. Upstream air masses' characteristics of northerly synoptic flows category, deduced from soundings at Toulouse.

IOP	Time of sounding mmddhh	FF (m s^{-1})	ϕ (deg)	V (m s^{-1})	$d\theta/dz$ (°C/100 m)	$N\cdot 100$ (s^{-1})	Fr $\frac{V}{NH}$	Ro $\frac{V}{fa}$	Fr/Ro $\frac{fa}{NH}$	P. W. cond	D (Pa)
1	100417	04.4	45	03.1	0.5	1.3	0.08	0.78	0.10	4b	5.03
	100423	08.4	−36	06.8	0.6	1.4	0.16	1.70	0.09	4a	5.09
	100505	10.0	−24	09.1	0.6	1.4	0.22	2.28	0.10	4a	4.14
	100511	12.8	−08	12.7	0.5	1.4	0.30	3.18	0.09	4a	3.80
	100517	09.0	05	08.9	0.6	1.4	0.21	2.23	0.09	4a	3.63
6	110317	07.5	−73	02.2	0.3	1.0	0.07	0.55	0.13	4b	2.02
	110323	07.3	−71	02.4	0.3	1.1	0.07	0.60	0.12	4b	2.17
	110405	07.7	−59	03.8	0.4	1.3	0.10	0.95	0.11	4b	2.04
	110411	05.6	−44	04.0	0.4	1.2	0.11	1.00	0.11	4a	2.30
	110417	15.4	−60	07.7	0.4	1.2	0.22	1.93	0.11	4a	2.37
	110423	09.6	−52	05.9	0.5	1.3	0.16	1.48	0.11	4a	1.50
	110506	07.3	−57	04.0	0.5	1.3	0.10	1.00	0.10	4a	0.83
	110511	05.4	−65	02.3	0.5	1.3	0.06	0.58	0.10	4b	0.60
8	111123	11.3	−45	08.0	0.6	1.4	0.19	2.00	0.10	4a	0.18
	111205	14.2	−42	10.6	0.6	1.4	0.25	2.65	0.09	4a	2.30
	111211	12.1	−17	11.6	0.6	1.4	0.28	2.90	0.10	4a	2.33
	111217	10.3	−27	09.2	0.6	1.4	0.22	2.30	0.10	4a	1.40
9	111405	12.3	−72	03.8	0.5	1.4	0.09	0.95	0.09	4b	1.72
	111411	20.2	−70	06.9	0.5	1.3	0.18	1.73	0.10	4a	2.29
	111417	19.6	−53	11.8	0.5	1.3	0.30	2.95	0.10	4a	5.65
	111423	17.8	−49	11.7	0.5	1.3	0.30	2.93	0.10	4a	4.45
	111505	19.0	−58	10.1	0.5	1.4	0.24	2.53	0.09	4a	3.88
	111511	20.9	−47	14.3	0.5	1.3	0.37	3.58	0.10	4a	4.88
	111517	21.2	−35	17.4	0.5	1.4	0.40	4.35	0.09	4a	6.27
	111523	21.7	−25	18.4	0.6	1.4	0.44	4.60	0.10	4a	6.69
	111605	17.0	−18	16.2	0.6	1.4	0.39	4.05	0.10	4a	6.32
	111611	14.8	01	14.8	0.6	1.4	0.35	3.70	0.09	4a	6.25
	111617	11.8	−05	11.7	0.5	1.4	0.28	2.93	0.10	4a	5.22
10	112823	04.7	11	04.6	0.3	1.1	0.14	1.15	0.12	4a	1.87
	112905	06.7	03	06.7	0.4	1.2	0.19	1.68	0.11	4a	2.09
	112911	06.8	30	05.9	0.4	1.2	0.16	1.48	0.11	4a	2.56
	112917	07.0	17	06.6	0.4	1.3	0.17	1.65	0.10	4a	2.88
	112923	09.4	−20	08.8	0.5	1.4	0.21	2.20	0.10	4a	3.10
	113005	13.0	−29	11.2	0.5	1.3	0.29	2.80	0.10	4a	5.12
	113011	13.4	07	13.6	0.5	1.3	0.35	3.40	0.10	4a	6.58

1991) and demonstrated that the extrapolation of the linear theory to nonlinear airflow around a circular barrier can provide a good description of the main characteristics of the horizontal blocked flow, in front and in the lateral borders of the mountain. These results encouraged us to use the linear theory to analyze the data collected in the PYREX experiment around the Pyrénées, even in the event that the flow is blocked and the regional winds detected during the IOPs between ground level and an altitude smaller than the mountaintop are generated mainly by the splitting of the air around the mountain range (i.e., no hydraulic jump, etc.). In particular, we found it worthy to relate the regional winds around the mountain range to the dynamic properties of the incoming air masses, characterized by Froude and Rossby numbers and the direction of incidence (DI) of the undisturbed mean wind, since simple numerical models based on the linear theory can be easily implemented in pure and applied research and operational tasks.

To follow the methodology used in mathematics when a statement ''if and only if'' is to be proved, the link between the experimental results collected in PYREX and the linear theory is presented in two parts. Part I describes, in general terms, the formation of the regional winds in the flanks of the Pyrénées, subjected to the influence of the upwind airmass characteristics and the perturbed pressure field. The experimental data are then used to asses some of the predictions of the extrapolation of the linear theory to the cases under study. To do that, the Froude number is adopted as the key tool due to its explicit role in some expressions derived from the manipulation of the linearized equations. In Part II (Koffi et al. 1998), the linear model developed by Smith (1980) is adapted to take into account the Coriolis effect, the DI, and elliptic mountains that resemble the Pyrénées. The influence of the Rossby number on the total pressure and wind intensity fields is evaluated. Then, the applicability of the extrapolation of this linear model, to explain the main features of blocked airflow with a relatively low Froude number, is tested by comparing numerical simulation results to the data measured during the PYREX experiment, where induced winds appear to develop. It should be remarked that the analysis of

TABLE 1b. Upstream air masses' characteristics of southerly synoptic flows category, deduced from soundings at Zaragoza.

IOP	Time of sounding mmddhh	FF (m s^{-1})	ϕ (deg)	V (m s^{-1})	$d\theta/dz$ (°C/100 m)	$N\cdot 100$ (s^{-1})	Fr $\frac{V}{NH}$	Ro $\frac{V}{fa}$	Fr/Ro $\frac{fa}{NH}$	P. W. cond	D (Pa)
2	101217	6.2	193	−06.0	0.4	1.2	0.17	1.50	0.11	4a	−2.93
	101223	8.9	183	−08.9	0.4	1.2	0.25	2.23	0.11	4a	−3.23
	101311	7.9	225	−05.6	0.4	1.3	0.14	1.40	0.10	4a	−1.75
	101317	9.0	232	−05.6	0.4	1.2	0.16	1.40	0.11	4a	−1.42
	101323	8.7	222	−06.5	0.4	1.2	0.18	1.63	0.11	4a	−1.85
	101405	8.9	213	−07.5	0.4	1.2	0.21	1.88	0.11	4a	−0.71
3	101411	8.0	193	−07.7	0.4	1.2	0.21	1.93	0.11	4a	−1.72
	101423	14.8	168	−14.3	0.4	1.3	0.37	3.58	0.10	4a	−4.36
	101501	16.8	180	−16.8	0.4	1.2	0.47	4.20	0.11	4a	−4.10
	101505	16.6	194	−16.1	0.4	1.2	0.45	4.03	0.11	4a	−5.33
	101511	16.1	185	−16.0	0.3	1.1	0.50	4.00	0.13	4a	−5.45
	101517	14.0	188	−13.7	0.3	1.0	0.46	3.43	0.13	4a	−2.48
	101523	10.8	208	−09.5	0.3	1.0	0.32	2.38	0.13	4a	−1.32
4	102018	9.3	186	−09.2	0.4	1.2	0.26	2.30	0.11	4a	−1.88
	102023	11.2	204	−10.2	0.5	1.3	0.26	2.55	0.10	4a	−2.71
	102105	12.4	213	−10.4	0.5	1.3	0.27	2.60	0.10	4a	−1.77
	102113	11.4	184	−11.4	0.4	1.2	0.32	2.85	0.11	4a	−0.54
	102117	13.0	177	−12.7	0.4	1.2	0.35	3.18	0.11	4a	−1.18
5	102423	11.0	250	−03.7	0.4	1.1	0.11	0.93	0.12	4b	−0.20
	102505	18.3	243	−08.3	0.4	1.2	0.23	2.08	0.11	4a	−0.21
	102511	10.6	253	−03.1	0.4	1.1	0.09	0.78	0.12	4b	−1.39
	102517	13.2	250	−04.5	0.4	1.1	0.14	1.23	0.11	4a	−2.60
7	110617	5.6	223	−04.1	0.4	1.3	0.11	1.03	0.11	4a	−1.39
	110623	6.0	208	−05.2	0.5	1.3	0.13	1.30	0.10	4a	−1.95
	110705	5.5	196	−05.3	0.5	1.3	0.14	1.33	0.11	4a	−2.33
	110717	7.5	172	−07.4	0.4	1.3	0.19	1.85	0.10	4a	−3.60
	110723	9.8	181	−09.8	0.5	1.3	0.25	2.45	0.10	4a	−4.61

FF, wind intensity; ϕ, direction of incidence of the undisturbed incoming flow, measured clockwise from the axis normal to the Pyrénées; V, normal wind component; $d\theta/dz$, potential temperature gradient; N, Brunt–Väisälä frequency; Fr, V/NH—Froude number; Ro, V/fa—Rossby number at altitude 3000 m; P. W. cond, Pierrehumbert and Wyman (1985) condition for blocked airflow, as specified by Eqs. (4a) and (4b) in the text; H, 3000 m—top height of the Pyrénées; a, 40 km—half-width of the Pyrénées; f, 0.0001 s^{-1}—parameter of Coriolis; D, pressure drag per unit area (Davies and Phillips 1985; Bessmoulin et al. 1993).

the deviations from the main features in particular cases is left out of the scope of this work and that the application of a rigorous methodology is only schematic and dedicated to provide a suitable framework for the presentation of the topic.

2. Brief description of the PYREX field experiment

a. Description of the area

The PYREX experiment (Bougeault et al. 1990) was launched by the French and Spanish meteorological services. The experimental field program was carried out from 1 October to 30 November 1990 and focused on the study of the influence of the Pyrénées range on the atmospheric dynamic flow. The principal objective of PYREX was to quantify the different terms of the momentum budget over the Pyrénées range, modified by friction, mountain waves, and secondary flows (deflected winds). The Pyrénées were chosen for the experimental program on account of their relatively simple shape. The range extends 400 km along the French–Spanish border, from the Atlantic Ocean to the west to the Mediterranean Sea to the east, and has a varying width of 40 to 80 km and a maximum altitude of 3000 m above mean sea level (MSL) in its central part. The geographical orientation of the Pyrénées, idealized by an ellipsoid, is indicated in Fig. 1, relative to north. Additional mountain ranges are present around the Pyrénées: to the northeast is the Massif Central with the Montagne Noire, and to the south, the Ebro valley separates the Pyrénées from the Iberic range (whose height does not exceed 1500 m), prolonged by the Cantabric range to the west. In fact, the whole mountain range forms an important barrier to northerly and southerly synoptic flows (Fig. 2a).

Figure 2b shows a three-dimensional view of the Pyrénées from the northwest. The topography is flat in the Bassin Aquitain to the northwest, while to the northeast, there is a constriction between the Pyrénées and the Montagne Noire at the Naurouze Path. The Pyrénées are extended westward by the Cantabric range. The topography on the east side facing the northerly flows is sharply defined, in opposition to the western side. Southerly synoptic flows are strongly disturbed by the mountainous areas upstream of the Pyrénées, that is, the Plateau of Castilla, Guadarama range, Iberic range, and the Ebro valley. The deflection area on the east edge is less

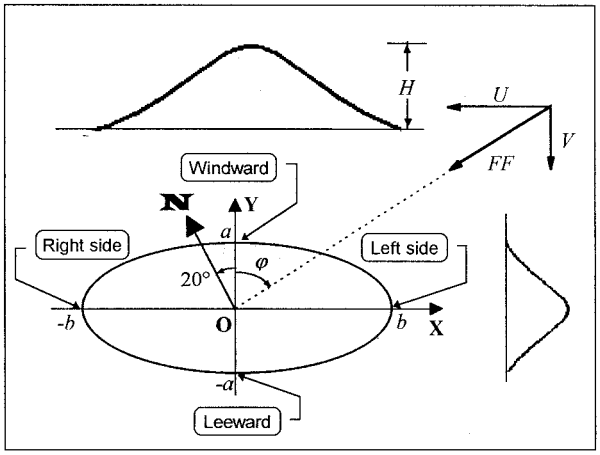

FIG. 1. Schematic representation of the Pyrénées by a topographic barrier having an elliptical horizontal cross section with aspect ratio $\gamma = a/b = 1/5 = 0.2$. The coordinate system is rotated 20° eastward from north, same as in the Pyrénées range.

disturbed by additional topography than in the west. On the French side, the wake of southerly flows can be perturbed by the Montagne Noire.

It is common to define the airflow around a topographic obstacle as the superposition of the mean incoming flow and a perturbation due to the interaction of the incoming flow with the barrier. A reference system is normally attached to the topographic obstacle to be used for the definition and the manipulation of the geometric and dynamic parameters involved in the flow. The particular shape of the Pyrénées can be idealized by a centered ellipsoid in an *XOY* coordinate system, having principal axis 2*b* oriented in the *X* direction and secondary axis 2*a* oriented in the *Y* direction, that is pointing about 20° east from north (Fig. 1). By convention, angles are measured clockwise from the positive direction of *Y* axis. The DI of the incoming flow (φ) is defined as the angle of the vector pointing to the incoming flow direction. The incoming wind components in the *X* and *Y* directions, which are parallel and normal to the principal axis of the mountain, will be represented by *U* and *V*, respectively. For each sounding used to characterize the incoming flow, it will be assumed that *U* and *V* remain constant and, consequently, $\tan\varphi = U/V = \text{constant}$.

The aspect ratio γ defined in Eq. (1) can be estimated to be one-fifth for an elliptical mountain profile idealization of the Pyrénées (Koffi et al 1998).

b. The experimental setup

The experimental setup put in operation in PYREX is fully described in Bougeault et al. (1993) and will be briefly mentioned here. It included 11 radiosonde sounding sites, several networks of automatic weather stations, constant volume balloons launched from three locations, four sodars, three wind profilers (ST radar),

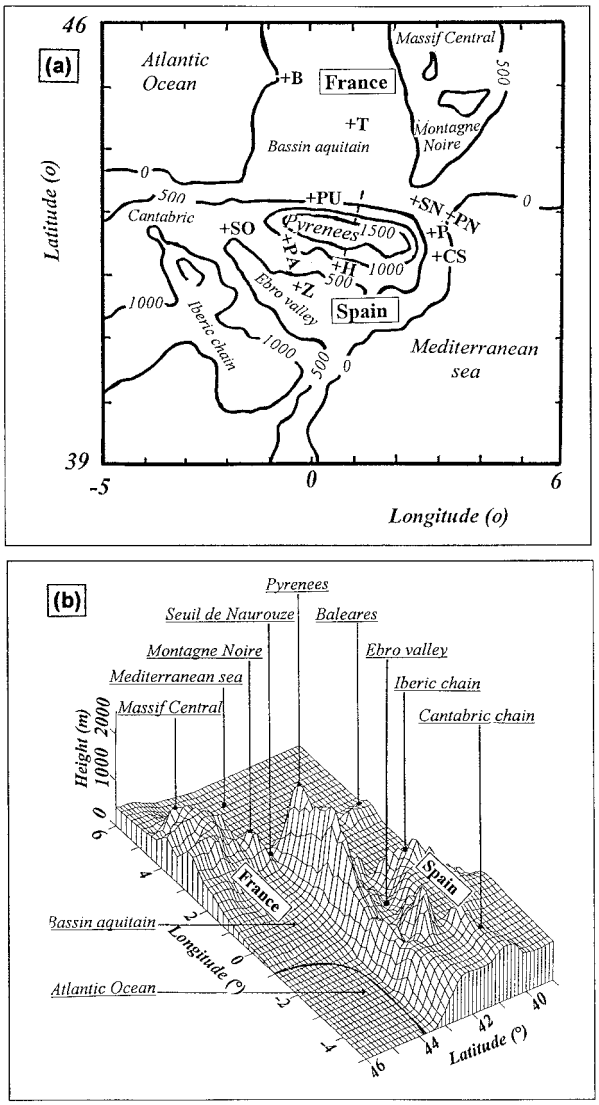

FIG. 2. Two views of the geographical domain of PYREX experiment activities, based on the 3D grid used in the PERIDOT model. (a) Map of the Pyrénées area showing major topographic features and relevant measurement sites, indicated by +**B** for Bordeaux, +**T** for Toulouse, +**SN** for Seuil de Naurouze (Naurouze Path), +**PN** for Port la Nouvelle, +**P** for Perpignan, +**CS** for Cap Creus, +**PU** for Pau, +**SO** for Sondica, +**PA** for Pamplona, +**Z** for Zaragoza, and +**H** for Huesca. (b) 3D plot including locations of interest, viewed from the north (French) side.

and four research aircraft (one of them carrying a backscattering lidar). Pressure was measured continuously during PYREX, using a network of microbarographs located along the *Y* axis on both sides of the mountain (Bessemoulin et al. 1993) and automatic weather stations spread around the Pyrénées. The relevant wind data used in the present paper was collected by the radiosondes, three French aircraft (Fokker 27, Merlin IV, and Piper Aztec), two sodars located in the Naurouze Path and in Zaragoza in the Ebro valley, and constant volume balloons (CVBs) launched from Port la Nou-

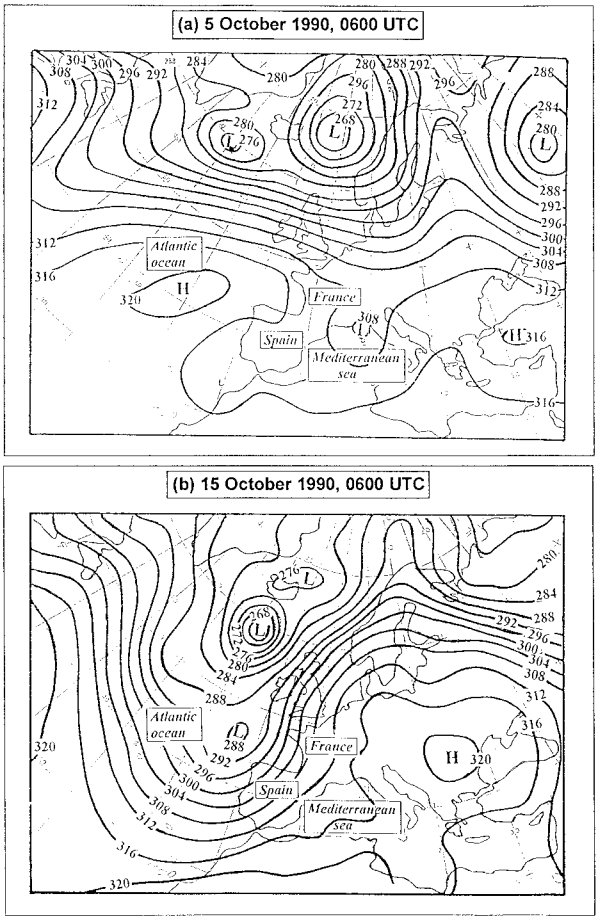

FIG. 3. Synoptic charts of 700-hPa isohypses at 0600 UTC for (a) northerly synoptic flow case on 5 October 1990 and (b) southerly synoptic flow case on 15 October 1990.

velle or Cap Creus (Fig. 3a). The temperature profiles of the incoming air masses were collected by the radiosondes. The experimental database analyzed in the present paper is that collected mainly by aircraft and CVBs between 200 and 600 m MSL, sodars between 100 and 200 m MSL, and radiosondes from ground level up to the tropopause. The precision of the horizontal wind is estimated to be 0.5 m s^{-1} and of the temperature 0.2 K.

c. Operational program

The measurements during the PYREX experiment were concentrated in 10 IOPs, which mode for 15 days of interesting meteorological conditions, to study the objectives of the experiment. The present cases will be classified in two synoptic flow categories: nine *northerly synoptic flows* documented in five IOPs and six *southerly synoptic flows* documented in five IOPs (see Table 1 in Bougeault et al. 1993).

3. Incoming airmass characteristics

It is assumed that the incoming flow can be completely characterized by the synoptic pressure field, the thermodynamic parameters, and the dimensionless numbers defined in Eqs. (2) and (3), as observed in the undisturbed zone upstream from the mountain range. Numerical (Stein 1992) and laboratory (Hunt and Snyder 1980) experiments showed that at lower layers horizontal blocked flows are split at a distance of the barrier equivalent to 1.2 to 2.4 times its half-width. Therefore, since the half-width of the Pyrénées is about 40 km, Toulouse (120 km to the north) and Zaragoza (100 km to the south) were considered the best of all the available soundings stations to be used to characterize the incoming air masses for northerly and southerly synoptic flows, respectively (Fig. 2a). The average values of the parameters that characterize the incoming flows, measured at both stations, are presented in Tables 1a and 1b, respectively.

a. Synoptic pressure field

The meteorological conditions inducing regional winds around the Pyrénées correspond to synoptic flows nearly normal to the Pyrénées principal axis, that is, dominant northerly or southerly components. Northerly flows at relevant altitudes (700 hPa) can occur when an anticyclone is present over the Atlantic Ocean and a low pressure system is in the western Mediterranean Sea, as illustrated in Fig. 3a for IOP 1 on 5 October 1990. Southerly flows are associated with a low pressure system over the North Atlantic Ocean and an anticyclone to the east. An example is the synoptic situation found in IOP 3, characterized by a low pressure zone located over the North Atlantic and a high pressure system centered east of the Black Sea (Fig. 3b). In both cases the isohypses are almost perpendicular to the mountain range.

b. Wind characteristics

A basic assumption made for the development of the linear model used to analyze the present data (Koffi et al. 1998) is that the wind profile is uniform. Because the preliminary analysis of the experimental data show that at low levels the flow regime at Toulouse and Zaragoza was affected by the blocking action of the Pyrénées, it was necessary to calculate a linear wind profile for each representative sounding. This was accomplished by using the integrals of the components of the wind between 400 m MSL and twice the maximum height of the mountain (6000 m MSL). Two examples of this linearization process applied to the normal component of the wind V are illustrated in Figs. 4a and 4c, for two soundings corresponding to the synoptic chart for northerly and southerly flows in Fig. 3, respectively. The values found at 3000 m MSL (Fig. 4, dashed line)

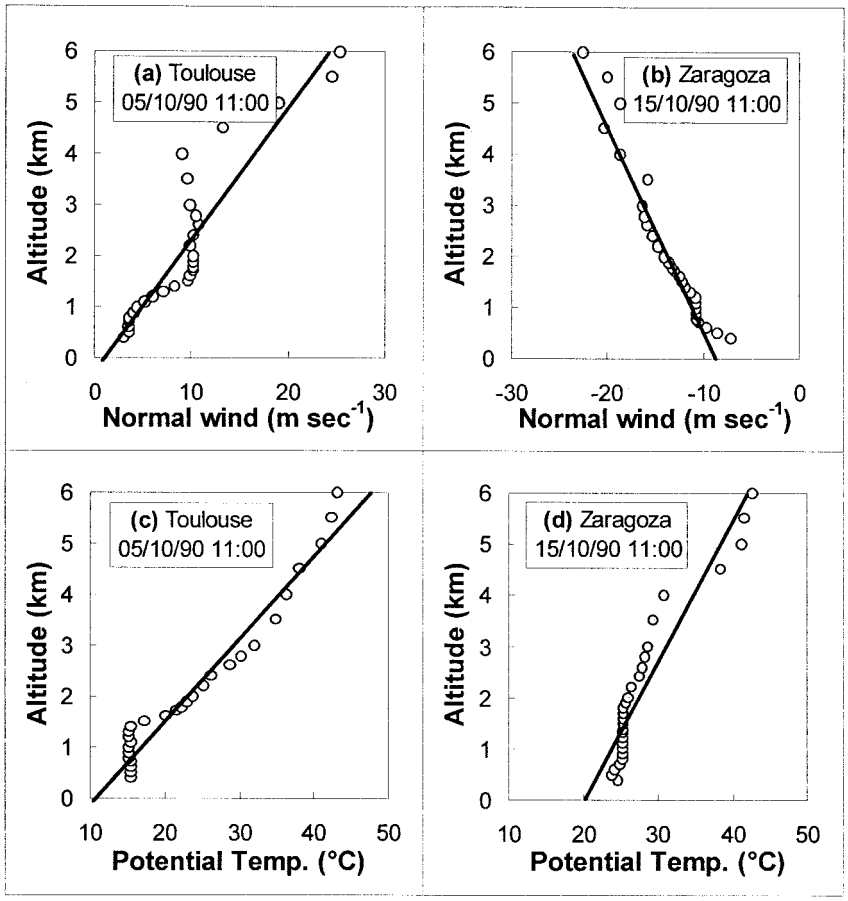

FIG. 4. The profiles of the normal wind component (a) and (b) and potential temperature (c) and (d) obtained from the radiosonde measurements (circular points) at 1100 UTC 5 October 1990 at Toulouse (a) and (c) for northerly flow and on 15 October 1990 Zaragosa (b) and (d) for southerly flow, and the linearized profiles (full line) used to obtain the characteristic parameters of the incoming air mass at 3000 m MSL (dashed line). The examples correspond to the synoptic charts in Fig. 3.

were used to define total velocity FF, normal component V, and DI φ of the incoming flow, as presented in Table 1. Wen-dar Chen and Smith (1987) and Spangler (1987) applied the same procedure from ground level up to the mountaintop. The integration interval adopted in the present analysis is found more appropriate because it rejects ground-level perturbations and, as Spangler (1987) showed, the characteristic parameters of the incoming flow, calculated between the ground and the mountaintop, are poorly correlated to the height of the separating layer between the lower and the upper flow.

Total wind velocity FF distributions for northerly and southerly categories (all the soundings) were found to be almost identical in almost all the cases in the range 10 to 20 m s^{-1}. Relatively light winds were found in IOPs 2 and 7.

Here, DI φ distributions for northerly and southerly categories were found to be different. In northerly flows, the DI vary between $-75°$ (westerly component) and 45° (easterly component), with considerable frequency in the range $-60°$ to $-30°$. The synoptic flow was consistently northeasterly only during IOP 10. In southerly cases, the departure of the incoming wind direction from normal incidence to the mountain range ($\varphi - 180°$) varies from $-15°$ (easterly component) to 75° (westerly component). Southeasterly synoptic wind directions were found sporadically only in four soundings.

The incoming wind normal component V distributions combine the behavior of the two preceding parameters. The normal component distributions for northerly and southerly categories were found to be similar. This fact does not contradict the difference in the distributions of φ because V is determined by $\cos\varphi$, which is an even function.

c. Thermal stability

The thermal stability is characterized by Brunt–Väisälä frequency N, defined by

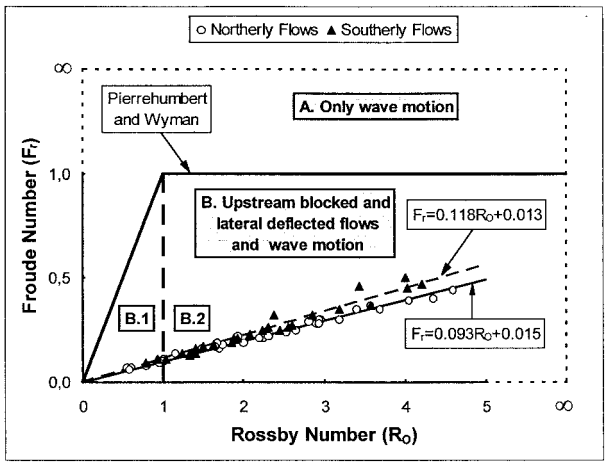

FIG. 5. Relationship between Rossby and Froude numbers measured in all the soundings performed in PYREX IOPs during northerly flows (empty marks) and southerly flows (filled marks) and the linear regression adjusted to northerly (solid line) and southerly (dashed line) flow categories. Pierrehumbert and Wyman (1985) diagram (heavy solid line) separates the graph into two flow regimes: "A" corresponds to mountain waves formation and "B" corresponds to upstream blocking effect. Subareas B.1 and B.2 correspond to Eqs. (4a) and (4b), respectively.

$$N = \left(\frac{g}{\theta_h}\frac{d\theta}{dz}\right)^{1/2}, \tag{5}$$

where g is the acceleration of gravity, θ_h the potential temperature, and $d\theta/dz$ the potential temperature gradient directly deduced from the linearization. Here, θ_h are the values found at 3000 m MSL (Figs. 4b and c, dashed line), following the same linearization procedure used for the wind, and exemplified in Figs. 4b and 4d for two soundings corresponding to the synoptic chart for northerly and southerly flows in Fig. 3, respectively. As the values of the thermal gradient shown in Table 1a [0.5 to 0.6 K (100 m)$^{-1}$] are, in general, greater than the values in Table 1b [0.3 to 0.5 K (100 m)$^{-1}$], the values of the Brunt–Vaïsala frequencies are consequently higher for the northerly category than for the southerly. Therefore, the flow in the former was, in general, more stable than in the latter.

d. Froude and Rossby numbers

The global dimensionless Froude (Fr) and Rossby (Ro) numbers are calculated by entering the values of N and V in Eqs. (2) and (3), respectively. Froude numbers were found to be lower than 0.5 for all PYREX IOPs, and Rossby numbers ranged between 0.5 and 5, but were generally greater than 1. The values of Fr and Ro in Tables 1a and 1b are plotted in Fig. 5, which includes the diagram of Pierrehumbert and Wyman [1985, Eqs. (4a) and (4b)] for comparison. PYREX data points are located in the sector of the graph corresponding to upstream blocking and splitting effects, which induce winds on the lateral edges of the obstacle. Good linear regression can be found for northerly and southerly flow data, demonstrating a linear dependence of Fr on Ro. This linear dependence indicates that the dynamic characteristics of the flows under study are mainly determined by the incoming wind, with the thermal stability and earth rotation playing a secondary role. The light difference between the slopes of the regression lines for northerly and southerly categories is induced by the thermal stability through N, which was shown to be almost constant, but different, for both flows.

4. Perturbation of the pressure field

Figure 6 displays two examples of ground-level pressure fields around the Pyrénées, interpolated from field measurements on 16 November 1990 (Fig. 6a) and on 15 October 1990 (Fig. 6b), at 0600 UTC (Bougeault and Mercusot 1992). The pressure values, measured at ground level, were reduced to mean sea level by the well-known standard method of using a lapse rate of 0.5 K (100 m)$^{-1}$. These figures illustrate the typical pressure perturbations, resulting from the blocking action of the Pyrénées range, on northerly and southerly incoming air masses, respectively.

When necessary in the following, the pressure perturbation will be analyzed using the *rate of change of pressure with distance* between two ground stations. The pressure measurements at ground level are reduced to sea level as explained above. This term will be symbolically represented by grad(p).

A second parameter that will be extensively used throughout this paper is the *pressure drag per unit area* (hereafter *pressure drag*) and is given by (Davies and Phillips 1985; Bessemoulin et al. 1993)

$$D = \frac{1}{L}\int_0^H \Delta p\, dz, \tag{5′}$$

where Δp is the pressure difference at each height z, along a segment of length L across the mountain. The integral, which accounts for the pressure difference across the mountain, is the *pressure drag per unit length of ridge* (Smith 1978). It is measured in units of force/length (N m^{-1}), while the drag per unit area in units of force/area = pressure (N m^{-2} = Pa). The pressure drag is computed using the pressure measured at ground level by 14 microbarographs located on a segment of length L = 150 km, which bisects the Pyrénées along the Y axis (x = 0) (Bessemoulin et al. 1993; Bougeault et al. 1993). By convention, the drag will be positive when the pressure increases from north to south and negative in the inverse sense. As can be seen in Table 1, northerly flows always have positive drag and southerly flows have negative. The variation range of the pressure drag for all the cases ranges from −6 to 8 Pa. The frequency distribution of the pressure drag is centered on 3 Pa and −2 Pa for northerly and southerly flows, respectively.

As pointed out previously, the total pressure field is a superposition of the synoptic pressure field and the

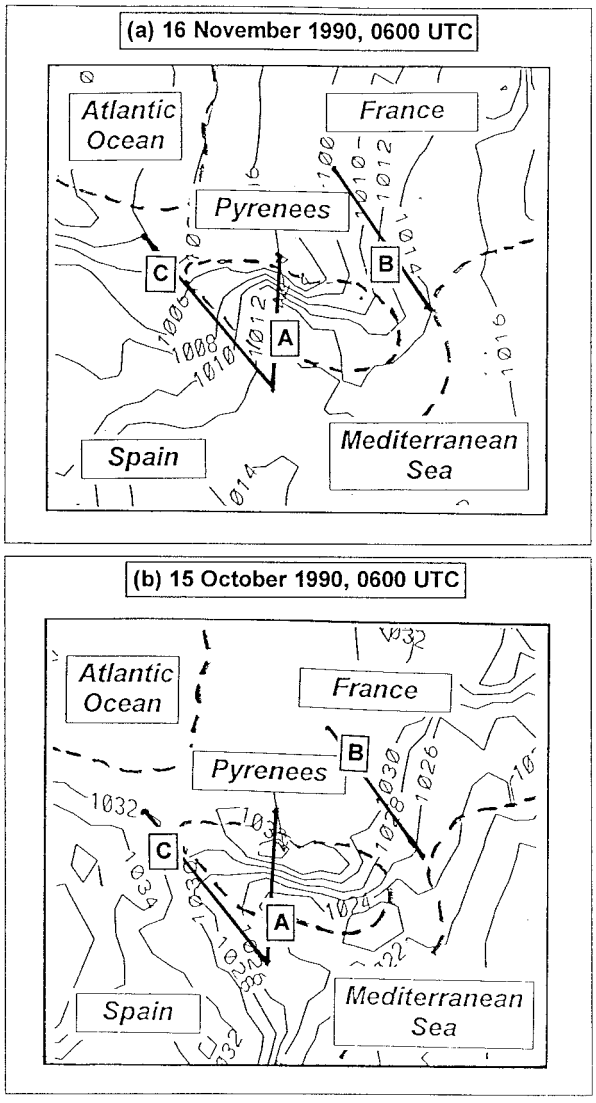

FIG. 6. Ground-level pressure maps deduced from the PERIDOT analysis at 0600 UTC for (a) northerly synoptic flow on 16 November 1990 during IOP 9 and (b) southerly synoptic flow on 15 October 1990 during IOP 3. The dotted lines indicate the location of the Pyrénées. Segment A joins the pair Pau–Zaragoza, B joins Toulouse–Perpignan, and C joins Zaragoza–Sondica.

pressure perturbations resulting from the blocking action of the mountain on the flow. It was difficult to discriminate the precise contribution of each term. To achieve a qualitative estimation of the synoptic contribution, the synoptic pressure gradient was calculated, assuming that the incoming flow, as defined in Table 1, is geostrophic. The values ranged from 0.01 to 0.02 hPa km^{-1} for the most frequent wind speed range of 10 to 20 m s^{-1}, respectively. For comparison, the pressure gradient was calculated for three pairs of ground stations: Pau–Zaragoza (X direction, segment A in Fig. 6), Toulouse–Perpignan (60° from X direction, segment B in Fig. 6), and Zaragoza–Sondica (45° from X direction, segment C in Fig. 6). For all the cases, the pressure gradient varies in the range from -0.05 to 0.05 hPa km^{-1}. Since the geostrophic pressure gradient direction is, in general, different from the orientation of the pairs of stations, it can be estimated that, on the average, the synoptic flow contribution to the perturbation pressure field is not greater than 30%. However, in some particular cases, the synoptic gradient can be more significant than the orographic perturbation. Considering the hefty assumptions made in the calculation, it was found unjustified to introduce this discrimination in the data processing.

The linear model of Koffi et al. (1998, Fig. 11) predicts that the pressure field resulting from the interaction of air masses moving toward an orographic barrier, having an elliptical cross section that resembles the shape of the Pyrénées, will exhibit an isobar constriction oriented along the mountain X axis. The general morphology of the pressure field shown in Fig. 6 resembles an orographic pressure dipole, with positive pressure perturbation values upstream of the mountain and negative pressure perturbation values downstream, in good agreement with this prediction.

The segments A, B, and C in Fig. 6 were chosen to have approximately the same length, and cut the same number of isobars, as predicted by the linear model developed by Koffi et al. (1998). The pressure rate of change along the segments were calculated for all the IOPs, and the results are plotted versus the corresponding pressure drags in Fig. 7, together with the lines of linear correlation calculated for northerly and southerly flows separately. The observed scattering of the data points should be attributed to the combination of experimental errors and the variability of the meteorological conditions during the different IOPs. For all the cases, the linear correlation coefficients are almost the same ($r \approx 0.8$), except for Toulouse–Perpignan (segment B in Fig. 6) during southerly flows ($r = 0.5$). The linear correlation for each pair of stations, calculated for northerly and southerly categories together, has a prevailing slope of about 0.55 km^{-1}. Due to the particular locations of the three pairs, the existence of such a prevailing slope can be interpreted as an experimental confirmation of the linear model results.

The slopes of the linear correlation are nearly equal to the prevailing slope for Zaragoza–Sondica (segment C in Fig. 6) during northerly and southerly flows and for Toulouse–Perpignan during northerly flows,. The individual slopes for Pau–Zaragoza (segment A in Fig. 6) differ from the prevailing slope by -20% for northerly flows and 25% for southerly flows. For Toulouse–Perpignan, the difference is -33% for southerly flows. Those differences can be attributed to the asymmetry of the mountain range, especially in the case of Pau–Zaragoza, which is located in the central part of the Pyrénées, and to an additional perturbation due to the particular orographic characteristic of the location of Perpignan for Toulouse–Perpignan.

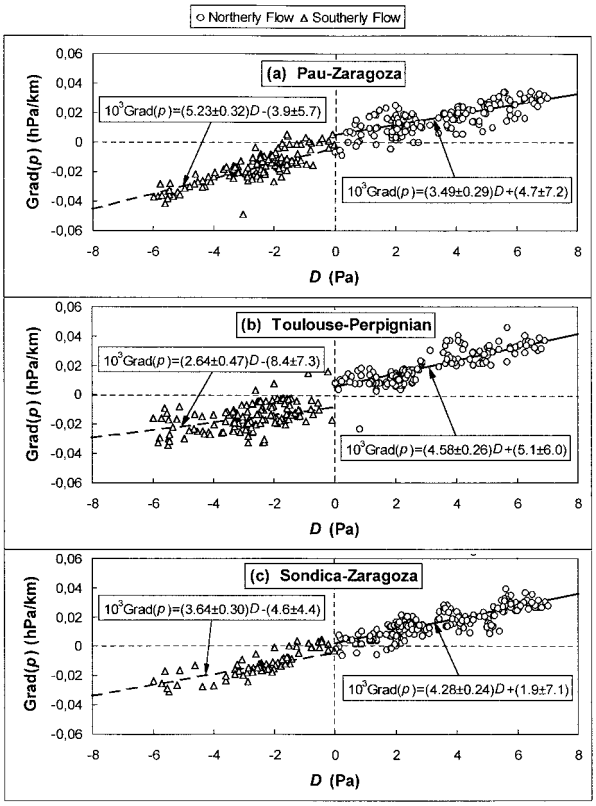

FIG. 7. Rate of change of ground-level pressure with distance between (a) Pau–Zaragoza (Fig. 6, segment A), (b) Toulouse–Perpignan (Fig. 6, and segment B), and (c) Sondica–Zaragoza (Fig. 6, segment C) vs pressure drag for northerly (circles) and southerly (triangles) flow categories. The linear regression adjusted to northerly (solid lines) and southerly (dashed lines) flow categories are also indicated.

From the analysis made above, it can be inferred that the correlation lines in Fig. 7 can be used to deduce the pressure perturbation around the Pyrénées directly from the measurement of the drag, as calculated in the present work. Inversely, the drag can be deduced from the rate of change of pressure with distance, measured between two stations located on both sides of the Pyrénées. A similar analysis has been reported by Bessemoulin et al. (1993). In consideration of its important role, the pressure drag will be used as representative of the pressure perturbation in the following sections.

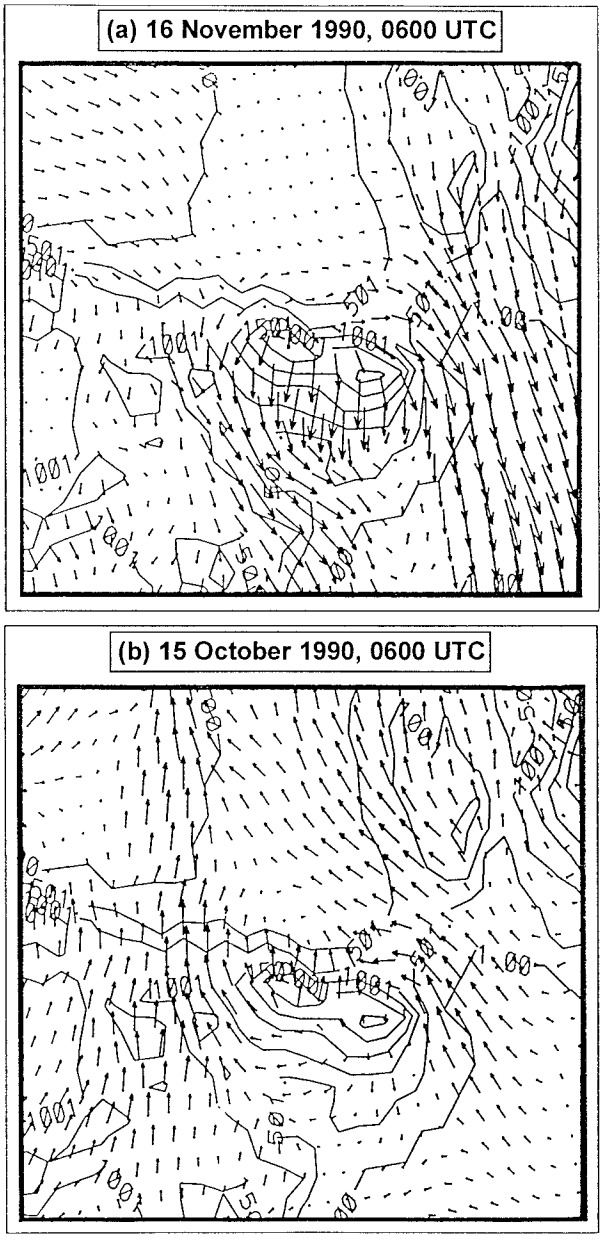

FIG. 8. Analysis of ground-level winds at 0600 UTC for (a) northerly synoptic flow on 16 November 1990 during IOP 9 and (b) southerly synoptic flow on 15 October 1990 during IOP 3 over a topographic map of the Pyrénées area.

5. Wind perturbation

The wind perturbations to be analyzed in the following sections concern the flow deflected by the blocking effect of the mountain range. These perturbations generate winds that are well known by their regional names. Two examples are demonstrated by the wind vector representation in Fig. 8, obtained using the PERIDOT numerical analysis of wind measurements performed at 0600 UTC 16 November 1990 (Fig. 8a) and on 15 October 1990 (Fig. 8b) during northerly and southerly synoptic flows, respectively. Figure 8 visualizes the main perturbations due to the blocking effect: flow retardation in front of the mountain, flow acceleration around the flanks, and vortex formation behind the barrier.

All the regional winds were observed during PYREX IOPs and were well characterized using the whole experimental setup presented above. In this section, they will be introduced briefly and, in the following section, they will be related to the pressure perturbation.

During northerly flows, the tramontane wind is in-

duced on the northeastern part of the Pyrénées, and the cierzo wind appears on the southwestern part (Fig. 8a).

Tramontane winds start between the Pyrénées and the Montagne Noire and blow over the Golfe du Lion in the Mediterranean Sea, reaching the maximum intensity offshore when they cross the prolongation of the *X* axis of the Pyrénées. The deflection is detectable up to altitudes of 1500–2000 m MSL, while the maximum intensity appears at 500 m MSL.

Cierzo winds start in the upper part of the Ebro valley and blow along it. The valley channels the horizontal flow at low levels and the maximum wind velocity is attained near Zaragoza. The deflection is detectable up to 2000 m MSL, and the maximum intensity is reached at altitudes between 500 and 1000 m MSL.

In southerly flow, the bochorno wind appears on the southwestern part of the Pyrénées, and the autan wind is induced on the northeastern part (Fig. 8b).

Bochorno winds blow in the upper part of the Ebro valley between Zaragoza and Pamplona; the maximum velocity is reached prior to the intersection with the *Y* axis of the Pyrénées. The deviated flow is detected from ground level up to 2000 m MSL.

Autan is the new name that marin winds receive over the Toulouse plain, after they originated by the splitting of the flow around the eastern part of the Pyrénées between Cap Creus and the Naurouze Path. They attain their highest velocity when they are accelerated by the bottleneck effect of the Naurouze Path. The deflection is detectable up to 1500–2000 m MSL, and the altitude of the maximum intensity is around 700 m MSL.

The *critical level of the blocked flow* h_c is, by definition, located at an altitude for which the perturbed motion of the air below is decoupled from the free motion of the incoming flow above. As pointed out above, in almost all the cases documented in the PYREX experiment, the horizontal wind field was found to be perturbed up to an altitude of 2000 m MSL. Therefore, this altitude, equivalent to two-thirds of the topographic barrier height, can be identified as the *critical level of the blocked flow* around the Pyrénées.

Hunt and Snyder (1980) have proposed to estimate the critical height in the blocking area using the equation

$$h_c = H(1 - \mathrm{Fr}). \tag{6}$$

Introducing in Eq. (6) the values $H = 3000$ m and $\mathrm{Fr} = 0.3$ that are representative for PYREX, one obtains $h_c = 2100$ m, in good agreement with the experimental values. A detailed analysis at Pau station, located in the blocking area of northerly flows, shows considerable scattering of the experimental data around the line given by Eq. (6), indicating that the dependence of the variation of h_c with Fr is more complex than stipulated by the equation, which does not account for all the experimental factors.

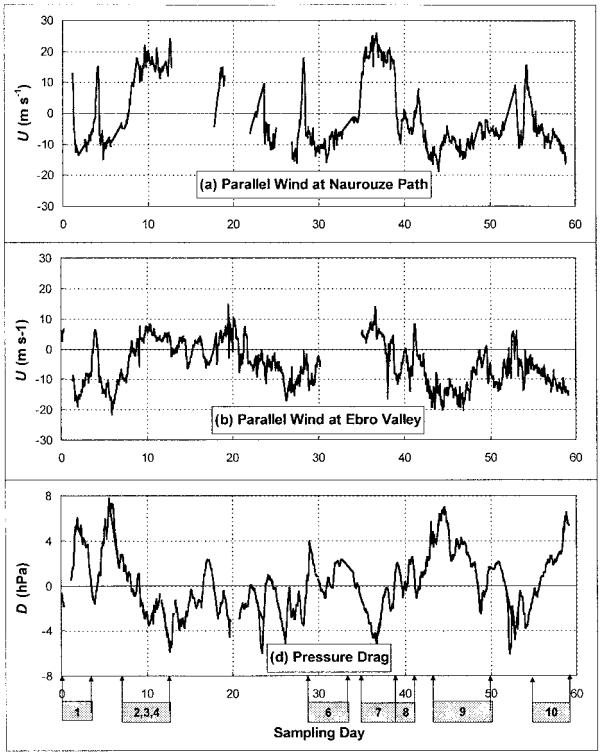

FIG. 9. Two-months time series of the total wind component parallel to the Pyrénées principal axis, as measured at 100 m AGL with sodars located at (a) Naurouze Path and (b) Zaragoza. (c) Same time series of the pressure drag. PYREX IOPs duration are indicated by the arrowed labels.

6. Wind and pressure interrelation

a. Temporal variation of the perturbed winds and the pressure drag

In general, a consistent direct positive or negative correlation between the pressure and the wind perturbations was observed during all PYREX operational periods. The good negative correlation is illustrated by the temporal variation of the pressure drag *D* and the parallel component of the wind *U*, measured in the Naurouze Path and at the Zaragoza airport, and is displayed in Fig. 9. When the synoptic flow is nearly perpendicular to the principal axis of the Pyrénées, the drag has significant values and the absolute values of *D* and *U* are in phase in both sides of the mountain. For synoptic airflow closely parallel to the principal axis of the Pyrénées, the drag is low and *U* fluctuates less systematically. A detailed analysis shows no significant time lag between the variations of the drag *D* and the *U* component of the wind, which is in agreement with the results of the cross correlation between the pressure perturbation index and the 900–800-hPa layer wind speeds for different lag times, as measured during the OLYMPEX experiment (Mass and Ferber 1990).

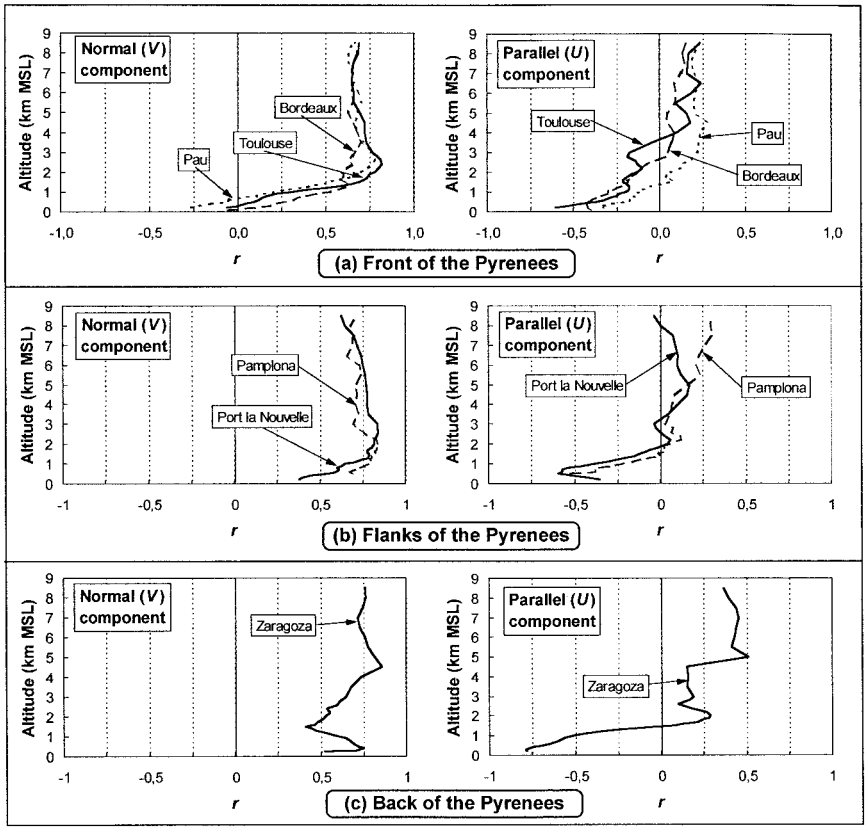

FIG. 10. Profiles of the coefficients of correlation between the pressure drag measured along a segment that bisects the Pyrénées, and the components of the total wind normal (left hand) and parallel (right hand) to the principal axis of the Pyrénées as measured by radiosondes deployed from stations located (a) in front, (b) at the edges, and (c) behind the mountain range, relative to the incoming flow direction, averaged for all IOPs with northerly flow.

b. Correlation between the wind profile and the pressure drag

Linear correlation coefficients between the wind components *V* and *U*, measured at several altitudes up to 8500 m MSL, and the pressure drag are shown in Fig. 10 for all the IOPs with northerly flows and in Fig. 11 for all the IOPs with southerly flows at seven stations (Koffi 1994). The stations were chosen to illustrate the conditions in front of the mountain range (Toulouse, Bordeaux, and Pau for northerly flow, and Zaragoza for southerly flow), behind the mountain range (the same stations but reversed), and at the edges (Pamplona is located on the west side, and Port la Nouvelle and Cap Creus are located on the east side of the Pyrénées). The significance level of the correlation coefficients shown in Figs. 10 and 11 are better than 0.1 in almost all the cases.

c. Analysis for northerly synoptic flows

The profiles of the linear correlation coefficients *r*, between the wind components and the pressure drag (Fig. 10a), are similar for all the frontal stations. Above 2000 m MSL the correlation coefficients for *V* are large ($0.7 < r < 0.8$), indicating that the pressure drag is mainly induced by the dynamic effect exerted by the mountain on the incoming flow. At Toulouse and Pau, the maximum correlation is found at altitudes between 2500 and 3000 m MSL, which can be considered representative heights of the mountaintops in the central part of the Pyrénées range. The correlation decreases for all the stations and inverts significantly only for Pau, at an altitude of 1000 m MSL, indicating the formation of an average reversing flow in the blocked zone below 2000 m MSL in front of the Pyrénées.

The correlation for the *U* wind component is weak above 2000 m MSL ($r < 0.3$), as expected from the analysis of the previous paragraph. Downward, the trend of the absolute values is to increase, contrarily to *V*, reaching significant values (0.4 to 0.6) near ground level. These negative correlation values indicate a prevailing westerly flow in the three frontal stations, as a result of the deflection of the flow toward the east.

The two main effects mentioned above are well established in Figs. 10b and 10c for the lateral (Port la Nouvelle and Pamplona) and rear (Zaragoza) stations:

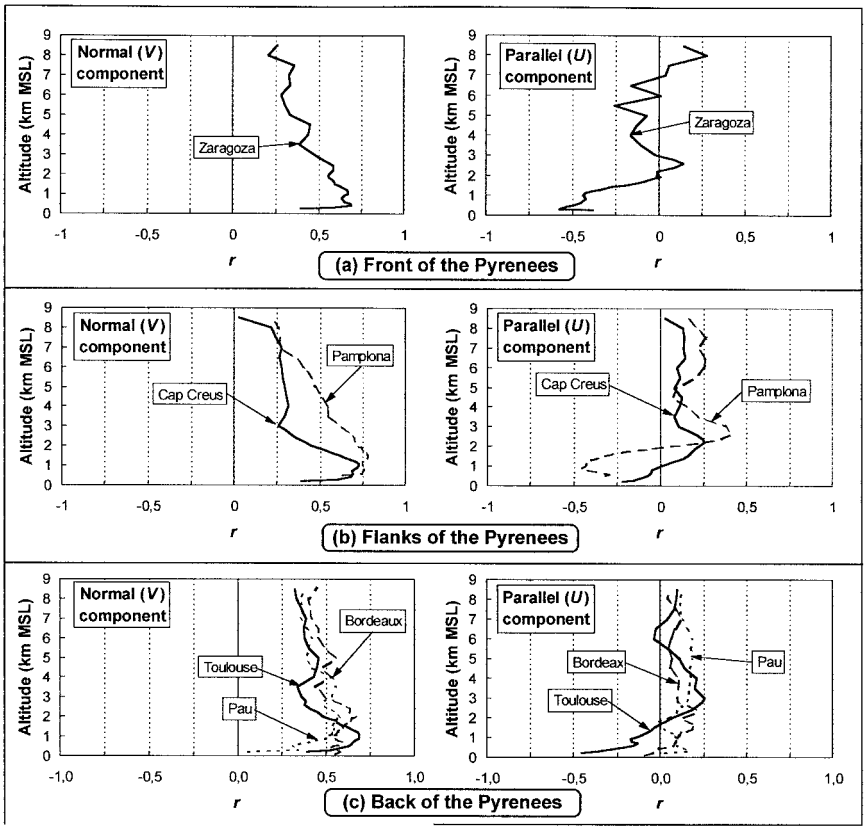

FIG. 11. Same as Fig. 10 for southerly flow category. The frontal and rear stations are inverted.

the free flow aloft (high correlation values of U above 2500 m MSL) and the eastward deviation on both sides of the Pyrénées (increasing absolute values of the correlation of V toward ground level).

Resuming the analysis of Fig. 10 above, the main features of the northerly flow can be described as follows. At a low level in front of the Pyrénées, somewhere westward from Pau, there is a point of strong deceleration in which the flow splits in two branches of westerly flow. A frontal branch starts up the tramontana wind (blocking effect), and a rear branch originates the cierzo wind (channeling effect of the Ebro valley). This flow pattern is in good agreement with the results obtained by Koffi et al. (1998) with a numerical model based on the linear theory that accounts for the Coriolis effect. Above the critical height defined heretofore, the horizontal flow is undisturbed. It should be remarked that the concept ''undisturbed flow'' regards the mean horizontal wind that was systematically measured, while the vertical wind component, which can be an indicator of wave formation and propagation, was measured only sporadically and is not analyzed here.

d. Analysis of southerly synoptic flows

The correlation between D and V decreases with altitude above 2000 m MSL, varying in the range $0.2 < r < 0.6$ (Fig. 11), indicating that southerly flows are more disturbed than northerly. While in Table 1 there are no considerable differences among DI, wind normal components, and drag statistical distributions for both categories, the stability is systematically lower for air masses coming from the south. This higher instability, combined with differences in topography, which is more complex on the Spanish side than on the French side of the Pyrénées, can explain the stronger perturbation in the upper levels. On the other hand, the fact that the trend of the correlation is, as for northerly flows, to keep on decreasing downward from 2000 m MSL and to reach its minimum value at ground level is an additional assessment of the existence of the separating critical level.

The correlation coefficient values for the U component of the wind vary irregularly between -0.2 and 0.3 above 2000 m MSL. Downward, they become negative, and the trend of their absolute values is to increase, reaching values in the range -0.2 to -0.6 near ground level, indicating a prevailing easterly flow caused by the deflection of the flow toward the west.

Resuming the analysis of Fig. 11, the main features of the southerly flow can be described as follows. At low level and in front of the Pyrénées, somewhere eastward from Zaragoza, there is a point of strong decel-

eration in which the flow splits in two branches of easterly flow: a frontal branch (blocking effect) starts up the bochorno wind, and a rear branch originates the marin and autan winds. This, again, resembles the results of the linear theory including the Coriolis effect (Koffi et al. 1998). Above the critical height, the horizontal flow is more disturbed than in the northerly flow.

The OLYMPEX experimental setup has provided a data bank that consisted mainly of radiosonde profiles from one sounding station at Quillayute, twice a day, and pressure charts from 11 microbarographs spread around the Olympic Mountain (Mass and Ferber 1990). The data collected and its analysis, which are of our immediate concern, are limited in two senses. First, a description of the three-dimensional wind field, statistically based on sounding stations surrounding the mountain, is not available. Second, the position of the microbarographs that provides the pressure perturbation index is unknown and, since the line connecting them cannot be a reference direction in space, any correlation with this parameter lacks direction. Therefore, the pictorial description of the flow pattern, as was presented above, cannot be attained. Nevertheless, the OLYMPEX experiment has shown that, on the average, the wind speed in the layers 900–700 hPa and 900–800 hPa is well correlated with the pressure perturbation index (Mass and Ferber 1990, Table 2 and Fig. 11). If the pressure perturbation index is accepted as a reasonable gauge of the pressure drag across the mountain, it can be inferred that our interpretation of the measurements performed around the elliptical-like Pyrénées range is in good agreement with the analysis gave by Mass and Ferber (1990) for the circular-like Olympic mountain.

The systematic wind-drag temporal correlation when $|D| > 2$ Pa (Fig. 9), and wind-drag space correlation (Figs. 10 and 11) around the mountain range for both incoming airmass categories, with special regards to the induced winds at low levels, enables the prediction of regional wind disturbances upheld by pressure drag observations. It will be shown that it can be linked to the dependence of both parameters on the Froude number, as predicted by the linear theory and confirmed by the experimental data. Under this conditions, the pressure drag becomes an accessible tool to forecast the important winds around the Pyrénées. This conclusion, subjected to a comprehensive experimental validation, can seemingly be extended to the Olympics, in view of the comparison made in the preceding paragraph.

7. Comparison of the experimental data with the linear theory

a. The pressure drag at the central part of the Pyrénées

The two-dimensional linear hydrostatic theory was elaborated to arrive to the dependence of the two-dimensional pressure drag per unit area $D_{2\mathrm{Dlin}}$ on Froude number given by Smith (1979a):

$$\frac{D_{2\mathrm{Dlin}}}{\rho_0 V^2} = \left(\frac{\pi}{4}\frac{H}{a}\right)\frac{1}{\mathrm{Fr}}, \tag{7}$$

where ρ_0 is the air density, and the others parameters were already defined. This relation shows that the two-dimensional pressure drag, normalized by $\rho_0 V^2$, is a linear function of Fr^{-1}. Equation (7) was extended to three-dimensional elliptical mountains by Phillips (1984):

$$D = D_{2\mathrm{Dlin}} G_1(\gamma, \varphi), \tag{8}$$

where the function $G_1(\gamma, \varphi)$ involves complicated elliptical integrals.

Following Phillips (1984) and Bessemoulin et al. (1993), Koffi et al. (1998) arrived at

$$D = D_{2\mathrm{Dlin}} G_2(\mathrm{Ro}, \gamma, \varphi), \tag{9}$$

which includes the Coriolis effect implicitly through Ro. The calculation of $G_2(R_0, \gamma, \varphi)$ also involves complicated elliptical integrals. Combining Eqs. (7) and (9), one obtains

$$\frac{D}{\rho_0 V^2} = \left(\frac{\pi}{4}\frac{H}{a}\right)\frac{1}{\mathrm{Fr}} G_2(\mathrm{Ro}, \gamma, \varphi). \tag{10}$$

To test these theoretical approaches, the absolute value of $D/(\rho_0 V^2)$ is plotted against Fr^{-1} in Fig. 12a, for all the PYREX IOPs (Table 1). A linear regression line for all the data, except four points that were rejected because they correspond to low Froude numbers, is also included in Fig. 12a. This rejection is consistent with the fact that the linear theory becomes less applicable for very small Froude numbers, as pointed out in the introduction. The correlation coefficient was 0.8, showing a strong linear correlation in general agreement with the linear theory. Using the coefficients of the regression line, one arrives to the empirical relation

$$\frac{D}{\rho_0 V^2} = (0.012 \pm 0.0013)\frac{1}{\mathrm{Fr}} - (0.014 \pm 0.023). \tag{11}$$

The data points in Fig. 12a are well grouped around the correlation line for $\mathrm{Fr}^{-1} < 8$. For $\mathrm{Fr}^{-1} > 8$, the data become more scattered, especially for IOP 6, which corresponds to a slow northwest synoptic flow associated with a low drag (three of the rejected points). This data point distribution is also in agreement with the criterion of linear theory validation, as mentioned above.

In Eq. (11), the free coefficient -0.014 is smaller than its standard deviation error (0.023) and can be ignored for a first approximation. In this case, the slope coefficient can be equated to the expressions deduced from Eqs. (7) and (10).

When the linear regression is compared to the two-dimensional linear approach (Eq. 7), one obtains

$$\left(\frac{\pi}{4}\frac{H}{a}\right) = 0.012. \tag{12}$$

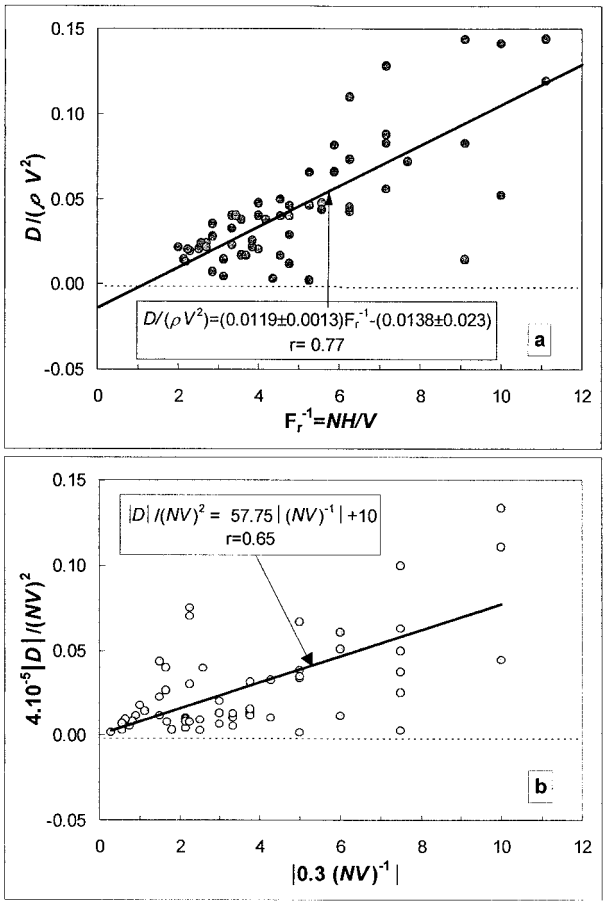

FIG. 12. Absolute value of the pressure drag as a function of the inverse Froude number for all PYREX IOPs, except four points having extremely high Froude numbers. The linear regression line is also shown.

From Eq. (12), it follows that $a = 65H$. After substituting $H = 3000$ m MSL, the representative height of the Pyrénées, in Eq. (12), the value $a = 195$ km is obtained, which is equivalent to 4.9 times the real width of the Pyrénées. In Koffi et al. (1998) it is shown that the perturbed pressure and wind area, calculated with a three-dimensional model for an idealized elliptic barrier having the same geometrical characteristics as the Pyrénées, extend to about 4.5 times the width of the barrier. Following this agreement, the value of a, calculated from Eq. (12), can be interpreted as the effective width of the Pyrénées, to be used in the implementation of models that rely on the two-dimensional linear theory that are dedicated to the study of the flow around this mountain range,

When the linear regression is compared to the three-dimensional linear approach [Eq. (10)], one obtains

$$\left(\frac{\pi}{4}\frac{H}{a}\right)G_2(\mathrm{Ro},\ \gamma,\ \varphi) = 0.012. \qquad (13)$$

The linear theory provides explicit mathematical expressions that enable the calculation of the function G_2 (Koffi et al. 1998), but its value is closely related to the definition and calculation of the parameters involved in its determination. For instance, the definition of the length of the microbarograph array that sustains the measured drag is an important factor that determines its value, not only because it appears in the denominator of Eq. (5) but also because the distribution of the drag along the segment is far from being uniform. Bessemoulin et al. (1993) has shown that the drag based on the 9 highest microbarograph located above 692 m MSL is about 40% higher than the drag calculated using the whole array of 44 microbarographs operated during PYREX. Based on the reduced array, the value of G_2 would have been 40% higher, namely, 0.0168. Since there is not a well-established methodology for the determination of the segment length, it remains an arbitrary subjective decision. The thermal stability that enters the calculation of G_2 as well as Fr through N depends to some extent on the linearization method applied to the experimental soundings for defining the characteristics of the uniform undisturbed flow. Olafson (1996) has proposed to linearize the ratio V/N if a wave formation is present, while for blocking and splitting effects he found it more appropriated to average V and N separately. Obviously, many other schemes can be applied, hat would increase the variability of the final value of G_2. Finally, we shall mention the definition of the geometry of the mountain as a source of subjective control on the value of G_2 by favoring a particular method of terrain smoothing. The smoothing scheme adopted by Koffi et al. (1998, Fig. 2) for PYREX is relatively well fitted to the terrain relief, which is in contrast to the dramatic spline simplification carried out by Davies and Phillips (1985, Fig. 3) to represent the orography of the St. Gotthard region, along the quasi-linear microbarographic array used in ALPEX experiment.

When G_2 is empirically obtained using the linear regression method applied in Fig. 12a, all the factors determining its value are globally embedded on it. In this sense, G_2 can be interpreted as a scaling function that enables one to obtain the pressure drag as a function of the Froude number, provided that the definition of the basic parameters of the dynamic system are kept fixed. The process developed above is a sort of experimental calibration of a particular aspect of the linear theory to be applied to a specific flow problem.

The linear theory developed by Smith and Phillips is conceptually controversial in the sense that it predicts flow features that are, in fact, nonlinear. Wave breaking, collapse of density surfaces, splitting, and stagnation of the flow are all effects that involve flow perturbations that are of the same order of magnitude, the average characteristics. Besides, clear criteria can be derived for the occurrence of such anomalies (Smith 1979b, 1980, 1988). The extent of the inaccuracies emanating from the anomalies introduced by the linearization process remained an aspect that should be examined in exper-

imental or numerical tests. The pressure drag, measured near the ground, is worth special attention, as will be shown below.

The series expansion of the density surfaces given by Smith's (1988) linear model in isosteric coordinates is rigorously correct at any point (x, y, z_0) for which $z_0N/V = (z_0/H)(HN/V) = (z_0/H)\mathrm{Fr}^{-1} < 0.5$, except in the wake of the hill, where the series converge poorly. Therefore, no matter how small the Froude number of the flow is, there will exist a layer of depth $z_0 < 0.5\mathrm{Fr}H$ above ground level for which the solution is rigorously valid in front and the flanks of the hill, and inaccurate in the wake. The validity and extent of the inaccuracies should be finally assessed by numerical and experimental tests.

We have arrived to the result that, under the experimental conditions and accuracies imposed by PYREX, the pressure drag can be related to relatively low Froude numbers in a way prescribed by the linear theory. We have sought other experiments to corroborate PYREX results, and we shall mention some relevant examples.

The data bank of the OLYMPEX experiment presented and analyzed by Mass and Ferber (1990) has two main limitations. First, as was pointed out previously, the pressure index can only poorly represent the pressure drag, as compared to its systematic measurement and the method in which it was calculated and analyzed in PYREX. Second, in spite of the expectations, the flow at Quillayute sounding station was, on the average, affected by the blocking effect of the Olympics, as is clearly demonstrated in Fig. 7 in Mass and Ferber (1990). If the wind direction at 700 hPa is accepted as representative of the incoming flow, only the wind entering the region parallel to the direction of the line connecting Quillayute with the Olympics (sector 280°–300° in the figure) is not deviated at lower levels. As the departure of the incoming flow from the line direction increases (sectors 240°–260° and 200°–220° in the figure), the wind deflection increases toward ground level (17° and 34° total average deflection, respectively), and it starts at higher levels (850 and 750 hPa, respectively), showing a more conspicuous splitting. An additional indication of the blocking effect at Quillayute is the deceleration of the flow. While the average wind speed at 700 hPa is almost the same for all the sectors, at 800 hPa it decreases to about 60% for sector 280°–300°, 80% for sector 240°–260°, and remains unaltered for sector 200°–220°, indicating that Quillayute moves the region of possible stagnation farther away as the splitting becomes more perceptible. Therefore, the Froude numbers calculated by Mass and Ferber (1990) cannot be representative of the normal incoming flow, as was applied in the present analysis. These two limitations may be a good explanation for the relatively poor pressure index–Froude number correlation found in OLYMPEX, which is in contrast to the results of our analysis of PYREX measurements. The fact that Quillayute is in the perturbed region can also explain that the wind velocity is the parameter that best correlates with all the others involved in the study of Mass and Ferber (1990).

ALPEX experimental drag determination, using pressure measurements along a 100-km-long quasi-linear array of microbarographs along the St. Gotthard Pass (Davies and Phillips 1985), is similar to the method used in the present analysis. The time variation of the drag per unit of area and the product NV during 2 months are given in Figs. 5 and 13, respectively, in Davies and Phillips (1985). The time series NV, based on sounding stations at Merenschwand and Milan for northerly and southerly flows, respectively, is incomplete and somewhat confusing. Nevertheless, it was possible to extract 78 paired values, which should be regarded as very inaccurate. The sole way to approach Fig. 12a using the data is to assume that N remains constant and the variation of NV is representative of the variation of V. Using NV instead of V to calculate the Froude number and $(NV)^2$ instead of ρV^2 to normalize the drag is a source of additional error that can be significant if the variation of N is $\pm 15\%$ as in PYREX (Table 1). Nevertheless, this procedure was applied to compose Fig. 12b, in which a pseudonormalized drag is plotted against a pseudo-Froude number, both arbitrarily scaled, to resemble the graph in Fig. 12a. Sixty-three out of the 78 original values were left, after the 15 outermost points were dropped, due to their extremely low Froude numbers. In spite of the adverse way that ALPEX data have to be treated, the similitude of the point distributions and the high valued correlation coefficients pertaining to PYREX and ALPEX is evident, and worth considering as an additional experimental corroboration of the functional dependence of the pressure drag on the Froude number prescribed by the linear theory when they are calculated and normalized as in the present analysis. The impossibility of calculating the average value of the scaling function G_2 for ALPEX conditions is regrettable, but this was caused by an inappropriate data format.

The modeling of two- and three-dimensional flows around mountain barriers, based on nonlinear equations, have contributed to some understanding of the dependence of the pressure drag on the Froude number. Miranda and James (1992) used a three-dimensional nonhydrostatic numerical model in terrain-following coordinates to study different flows around different circular bell-shaped mountains. They present a curve of the total pressure drag normalized by the linear hydrostatic drag as a function of Froude number, which shows a well-defined peak at $\mathrm{Fr} = 1$. Many substantial arguments enable the comparison of their results with PYREX experimental data, such as a) the mountain is kept circular while the Pyrénées range is best fitted by an elliptic shape having aspect ratio $\gamma = 1/5$; b) rotational, frictional, and turbulence effects are not included (experimental data cannot be cleared of these effects); c) the nature of the total drag, expressed in unit of force (N),

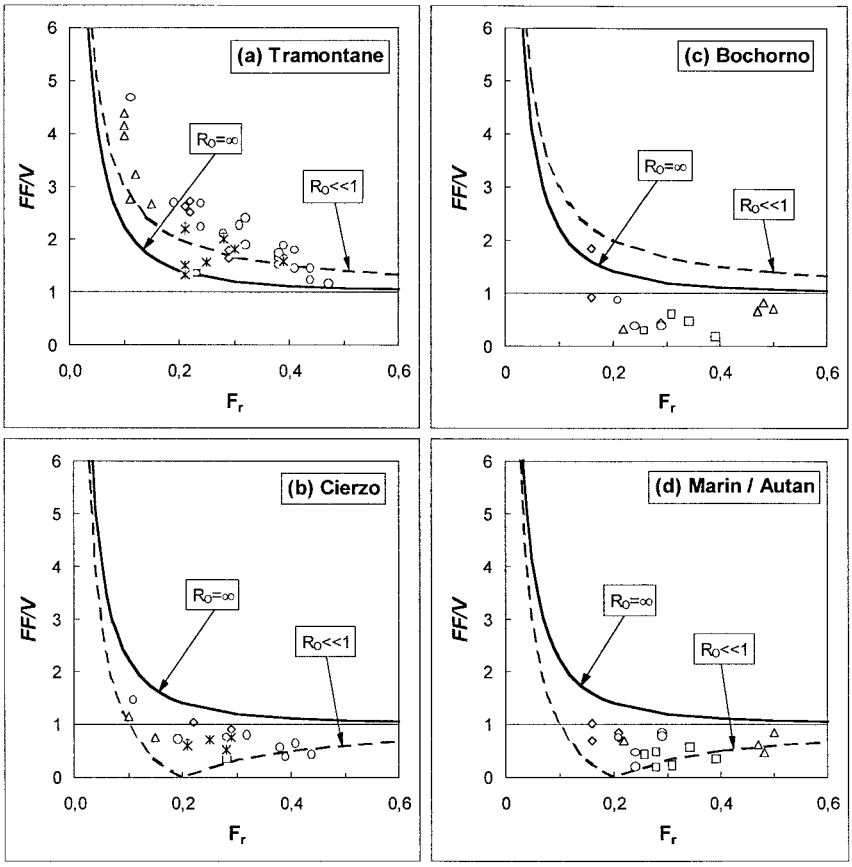

FIG. 13. The normalized total wind intensities at 500 m MSL as a function of the Froude number for northerly (a) and (b) and southerly (c) and (d) flow categories, deduced from measurements at (a) Port la Nouvelle and (d) Cap Creus on the east side and (b) and (c) Pamplona on the west slide of the Pyrénées. The solid line curve is deduced from Eq. (17) in the absence of the Coriolis effect (Ro = ∞), and the dashed line curve is deduced from Eq. (18) when the Coriolis effect is taken into account (Ro $\ll$ 1).

differs to a great extent from the drag per unit of area expressed in units of pressure (Pa), as was measured in PYREX and ALPEX. Ólafsson and Bougeault (1996) used a primitive equation in the hydrostatic, terrain-following coordinates, limited-area PERIDOT model, formerly operational at Météo-France, to simulate different flows around en elliptic mountain having $\gamma = 1/5$. Only turbulence effects were included. The drag per unit of area is calculated along a transect of 240 km and normalized by ρNVH^2. The curve of the normalized drag versus the inverse of Froude number has a well-defined peak at Fr = 1 and somehow resembles the curve of Miranda and James (1990, 1992), if the substantial differences between the experiment conditions are ignored and the abscise axis is inverted. PYREX conditions are better approached by Ólafsson (1996) and Ólafsson and Bougeault (1997) who, using the same modelization as Ólafsson and Bougeault (1996), also introduced rotation and friction. The effect obtained is impressive—the amplitude of the curves of the nondimensional drag per unit of area in the central part of the elliptical mountain, calculated with turbulence in the range $0.5 \leq \mathrm{Fr}^{-1} \leq 4.5$, are reduced by factors 0.74 when the Coriolis effect is introduced and by 0.42 when both rotation and friction effects are included. The reduction of the nondimensional total drag is even more noticeable: 0.56 and 0.28, respectively. This behavior is discussed in Ólafsson (1996) and Ólafsson and Bougeault (1997) and we shall not reproduce his argumentation. The flattening of those curves is equivalent to an approach to the linear drag behavior described in our formulation [Eqs. (9) and (10)]. The final adjustment of Ólaffson (1996) and Ólafsson and Bougeault (1997) curves to PYREX points remains a matter of scaling that is strongly dependent on the subjective parametrization, as explained previously.

b. Regional winds in the edges of the Pyrénées

In the present section, the experimental wind data measured near the western and eastern sides of the Pyrénées will be compared with the values on the edges of

an elliptical mountain, obtained by Buzzi and Tibaldi (1977) for Ro < 1 and $\gamma = 1$, Smith (1980) for Ro $= \infty$ and $\gamma = 1$, and Philips (1984) for Ro $= \infty$ and any γ, using models based on the linear theory.

In the linear theory, the total wind field is considered a superposition of the incoming flow (the average wind field) and the wind (the wind field perturbation). Using the coordinate system previously defined for a linear flow, the expression for the total wind velocity at ground level FF(x, y, 0), normalized by the normal component V of the incoming wind velocity taken at 3000 m MSL, is given by

$$\frac{\mathrm{FF}(x, y, 0)}{V} = \left\{\left[1 + \frac{v'(x, y, 0)}{V}\right]^2 + \left[\frac{U}{V} + \frac{u'(x, y, 0)}{V}\right]^2\right\}^{1/2}, \quad (14)$$

where $v'(x, y, 0)$ and $u'(x, y, 0)$ are the perturbations of the horizontal wind components. The wind perturbation for an incoming flow normal to the principal axis of the mountain range ($U = 0$, $\tan\varphi = 0$) and without Coriolis effect (Ro $= \infty$), calculated by Smith (1980) for a circular bell-shaped mountain ($\gamma = 1$) and by Phillips (1984) for a family of elliptical mountains (any γ), is

$$\left.\begin{aligned} v'(x, y, 0) &= -hNCp_{\gamma}(x, y, 0) \\ u'(x, y, 0) &= -hNCp_{1/\gamma}(x, y, 0) \end{aligned}\right\}, \quad (15)$$

where

$$\left.\begin{aligned} Cp_{\gamma}(x, y, 0) &= \frac{p'(x, y, 0)}{\rho_0 VNH} \\ Cp_{1/\gamma}(x, y, 0) &= \frac{p'_R(x, y, 0)}{\rho_0 VNH} \end{aligned}\right\}, \quad (16)$$

where $p'(x, y, 0)$ is the pressure perturbation in the presence of an elliptical terrain field $h(x, y)$, as defined in Koffi et al. (1998), and $p'_R(x, y, 0)$ is the pressure perturbation due to a terrain $h_R(x, y) = h(y, x)$, which is a reflection of the original barrier about the line $x = y$.

For normal incoming flows $U = 0$, the total wind velocities at the points ($\pm b$, 0, 0) are calculated, replacing the values $v'(\pm b, 0, 0) = 0$, $u'(\pm b, 0, 0) = -hNCp_{1/\gamma}(\pm b, 0, 0)$, and $\mathrm{Fr}^{-1} = NH/V$ in Eq. (14).

$$\frac{\mathrm{FF}(\pm b, 0, 0)}{V} = \left\{1 + \left[\frac{Cp_{1/\gamma}(\pm b, 0, 0)}{\mathrm{Fr}}\right]^2\right\}^{1:2}. \quad (17)$$

When the Coriolis effect is taken into account and Ro $\ll 1$, the flow in the vicinity of the mountain becomes quasigeostrophic. The wind velocity in the lateral edges of a circular mountain ($\gamma = 1$) is given by the following equation, deduced from Buzzi and Tibaldi (1977),

$$\frac{\mathrm{FF}(\pm b, 0, 0)}{V} = \left\{1 \pm \left[\frac{Cp_{1/\gamma}(\pm b, 0, 0)}{\mathrm{Fr}}\right]^2\right\}^{1/2}. \quad (18)$$

In Eq. (18), the plus sign preceding the ratio is for deflections leftward of the incoming flow direction and the minus sign is for rightward deflections. Equations (17) and (18) give the explicit dependence of the normalized total wind velocity on Fr on both sides of the mountain, when the flow is normal to the mountain range.

Figure 13 presents the experimental values of the ratio FF/V, measured between 100 and 500 m above ground level as a function of the Froude number, during the appearance of the tramontana and cierzo winds (Figs. 13a,b) and bochorno and marin–autan winds (Figs. 13c,d). The curves deduced from Eqs. (17) and (18) for normal incidence ($\varphi = 0$), using the respective values $Cp_{1/5}(\pm b, 0, 0) = 0.2$ and $Cp_1(\pm b, 0, 0) = 0.35$ given by Phillips (1984), are also plotted for comparison. In the absence of the Coriolis effect, the flow predicted by Eq. (17) on both sides of the barrier is symmetric, and the curves for Ro $= \infty$ are identical in all the cases. On the other hand, the asymmetry expected in Eq. (18) when the Coriolis effect is taken into account is reflected by the differences between the curves for Ro $\ll 1$ in Figs. 13a and 13c calculated with the positive sign, and in Figs. 13b and 13d calculated with negative sign.

In spite of systematic departures of the data points from the curves in Figs. 13a and 12c, it is clear that the experimental values are in general agreement with the linear theory predictions. Indeed, the distribution of the data points above the curves in Fig. 13a and below them in Fig. 13c is explained by the bias introduced to the flow by the synoptic wind that, on the average, bears 45° to the west of normal incidence for northerly as well as for southerly flow categories. During northerly flows, the DI provides a positive bias to the tramontana wind in Port la Nouvelle (east side of the Pyrénées) and a negative bias to the cierzo wind in Pamplona (west side of the Pyrénées). This bias enhances the asymmetry imposed to the flow by the Coriolis effect and is clearly demonstrated by Koffi et al. (1998) using the linear theory. However, the opposite tendency should be observed for the southerly category, where the linear theory predicts relatively weak wind perturbations for all the Fr corresponding to the data. But in this case, the systematic bias of the DI on the data is masked, probably because it is embedded in experimental errors and other dynamic effects.

The asymmetry mentioned above decays with altitude as shown in Fig. 14, which presents the averaged difference of the wind velocities in Port la Nouvelle (east side) and Pamplona (west side), for all IOPs of northerly and southerly categories (Fig. 14a,b, respectively). The standard deviations in Fig. 14 clearly demonstrate that the enhancement of the asymmetry due to the DI is significant for northerly flows (Fig. 14a), while the

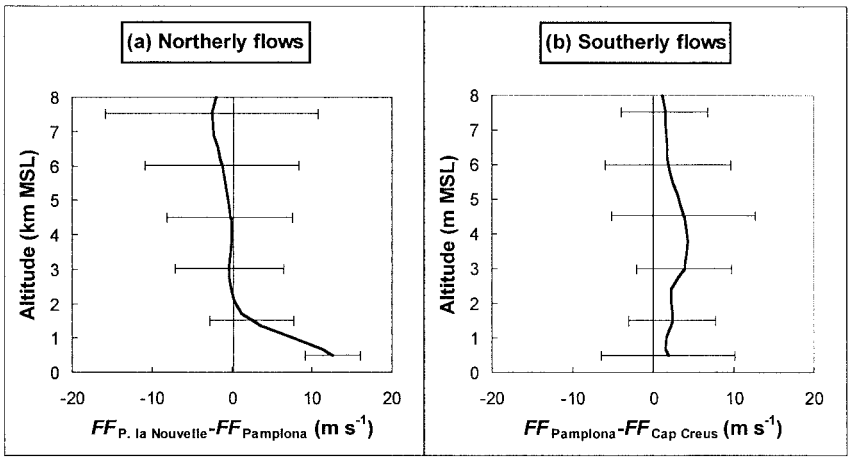

FIG. 14. Dependence on altitude of the difference of the total wind intensities between (a) Port la Nouvelle and Pamplona and (b) Pamplona and Cap Creus, for northerly and southerly flow categories, respectively. The horizontal bars represent the standard deviation of the measurements.

masking effect for southerly flow is composed in the error range (Fig. 14b). The error range at low levels is higher for the southerly than for the northerly flow because the winds during southerly flows were faster.

The decay of the flow asymmetry with altitude is an experimental confirmation of the declination of the mountain blocking effect with altitude, which is not attested by the implementations of the linear theory in Smith (1982), Philips (1984), and Koffi et al. (1998), but is demonstrated by Ólafsson (1996, Fig. 5.4) using the three-dimensional nonlinear PERIDOT model. While the critical level was previously identified and located in section 5 using the relation of Hunt and Snyder (1980) and in section 6b using the correlation between the wind and the pressure drag, the asymmetry decay in Fig. 14a is an additional and independent location of the critical level at about 2100 m MSL. Quantitatively, this estimation of the critical level altitude is in agreement with the values obtained previously, considering the error involved, as given by the standard deviations.

In fact, Fig. 14 synthesizes the main features of the flow in the vicinity of the Pyrénées: a separating layer between the air mass flowing with undisturbed horizontal direction above and the blocked flow below. The blocked northerly flow is asymmetric, with stronger wind velocities on the eastern side than on the western.

8. Conclusions

The PYREX intensive operational program had provided an extensive database, which was used in the present work to describe the airflow around the Pyrénées and to evaluate the applicability of the linear theory to stable flows, blocked by a relatively large mountain range.

The thermodynamic characteristics of incoming flows were defined in terms of Froude and Rossby numbers and the direction of incidence (DI) of the wind. Here, Fr and Ro were found linearly correlated and their combination corresponded to blocked flow in all the cases. The DI was used to classify all the cases in northerly and southerly incoming flow categories. In both categories, the incoming flow was not purely normal to the main axis of the mountain range, generally bearing to the west.

In the vertical direction, the flow is clearly separated into two regimes by a separating layer located at an altitude of about two-thirds of the way to the top of the mountain range. Above the separating layer, the horizontal wind is undisturbed. Below the separating layer, winds that are well known by their regional names are induced when the flow is perturbed by the blocking effect of the topographic barrier. Due to the wind perturbation, horizontal winds during northerly flows are stronger on the east side than on the west side, while during southerly incoming flows, the horizontal wind distribution is almost symmetric.

The pressure field perturbation is well correlated to the pressure drag, calculated along a segment bisecting the central part of the mountain range. Since the pressure drag was found to be correlated to the Froude number of the incoming flow, it was used to analyze the pressure field dependence on the dynamic interaction of the incoming flow with the mountain range.

Clear correlation rules can be deduced from the analysis of the experimental data at different altitudes for both categories of incoming flows. Therefore, since the pressure drag can be easily determined using field measurements at ground level, it becomes a powerful tool for the prediction of winds around the Pyrénées.

The experimental data are in agreement with the linear theory predictions as follows.

- The perturbation of the surface pressure field resembles a bipolar distribution with a high pressure system in front of the mountain and a low pressure system behind it.
- The dependence of the drag, measured in the center of the mountain, on Fr^{-1}. It was possible to evaluate the applicability of the linear theory implemented in two models—a two-dimensional model, for which it was possible to define quantitatively the effective blocked area, and a three-dimensional model, for which a scaling function that combines the DI, the mountain shape, and the Coriolis effect was found almost constant, with average value of 0.2 for all the cases under study.
- The extension of the area affected by the blocking effect, estimated to be 4.5–5 times the width of the barrier. For the northerly flow category, it was even possible to detect the rightward drift of the point of strong deceleration due to the Coriolis effect and to determine its location.
- The dependence of the wind velocities on Fr^{-1} at the edges of the barrier. The asymmetric deviation of the flow is clearly demonstrated for northerly flows, while for southerly flows it is considerably masked. The flow asymmetry is induced by the Coriolis effect and biased by the departure of the flow from normal incidence, toward westerly DI for both categories. As a result of the combination of both effects, the asymmetry is enhanced in northerly flows and reduced in southerly cases, as predicted by the linear model in Koffi et al. (1998). The feeble asymmetry in the southerly category is embedded in experimental errors and other dynamic effect.

Acknowledgments. The PYREX experiment was made possible by the participation of a large number of institutes and funding agencies. The participating institutes are CNRM, CRPE, LA, LAMP, LMD, LSEET, SA, EDF for France; INM, UV, UIB for Spain; and DLR for Germany. Funding was provided by Météo-France, INM, INSU (ARAT, PATOM, and PAMOY programs), CNES, EDF, DLR, and Région Midi-Pyrénées. Much technical help was provided by CEV, ENM, and the French and Spanish Air Force and air control authorities. We would like to express our gratitude to J. C. André, D. Cadet, D. Guedalia, and A. Ascaso Liria for their help in the planning of this program. We also would like to express our deep appreciation to the many colleagues who have participated to the success of the experiment through enormous personal commitment.

REFERENCES

Bessemoulin, P., P. Bougeault, A. Genoves, A. Jansa, and D. Puech, 1993: Mountain pressure drag during PYREX. *Beitr. Phys. Atmos.,* **66,** 305–325.

Bougeault, P., and C. Mercusot, 1992: Atlas des réanalyses PERIDOT de l'expérience PYREX. CNRM Note de Recherche 8, 104 pp. [Available from CNRM, Meteo France, 31057 Toulouse, France.]

——, A. Jansa, B. Bénech, B. Carissimo, J. Pelon, and E. Richard, 1990: Momentum budget over the Pyrénées: The PYREX experiment. *Bull. Amer. Meteor. Soc.,* **71,** 806–818.

——, B. Bret, P. Lacarrére, and J. Noilhan, 1991: An experiment with an advanced surface parametrization in a mesobeta-scale model. Part II: The 16 June simulation. *Mon. Wea. Rev.,* **119,** 2374–2392.

——, and Coauthors, 1993: The atmospheric momentum budget over a major atmospheric mountain range: First results of the PYREX program. *Ann. Geophys.,* **11,** 395–418.

Buzzi, A., and S. Tibaldi, 1977: Inertial and frictional effects on rotating and stratified flow over topography. *Quart. J. Roy. Meteor. Soc.,* **103,** 135–150.

Campins, J., A. Jansa, B. Bénech, E. Koffi, and P. Bessemoulin, 1995: PYREX observations and model diagnosis of the Tramontana wind. *Meteor. Atmos. Phys.,* **56,** 209–228.

Chen, W.-D., and R. B. Smith, 1987: Blocking and deflection of airflow by the Alps. *Mon. Wea. Rev.,* **115,** 2578–2597.

Davies, H. C., and P. D. Phillips, 1985: Mountain drag along the Gotthard section during ALPEX. *J. Atmos. Sci.,* **42,** 2093–2109.

Drazin, P. G., 1961: On the steady flow of a fluid of variable density past an obstacle. *Tellus,* **13,** 239–251.

Hunt, C. R., and W. H. Snyder, 1980: Experiments on stably and neutrally stratified flow over a model three-dimensional hill. *J. Fluid Mech.,* **96,** 671–704.

Imbard, M., A. Joly, and R. du Vachat, 1986: Le modèle de prévision numérique PERIDOT: Formulation dynamique et modes de fonctionnement. EERM Tech. Rep. 161, 41 pp. [Available from CNRM, 31057 Toulouse, France.]

Jansa, A., 1987: Distribution of the mistral. A satellite observation. *Meteor. Atmos. Phys.,* **36,** 201–214.

Koffi, E., 1994: Caractérisation expérimentale de l'écoulement atmosphérique autour d'un massif montagneux (Expérience Pyrex). Thése de doctorat 1764, Université Paul Sabatier, Toulouse, France, 258 pp. [Available from CRA, 65300 Lahnemezan, France.]

——, B. Bénech, J. Stein, and B. Terliuc, 1998: Dynamic characteristics of regional flows around the Pyrénées in view of the PYREX experiment. Part II: Solution of a linear model compared to field measurements. *J. Appl. Meteor.,* **37,** 53–71.

Lyra, G., 1943: Theorie der stationären Leewellenströmung in freier Atmosphäre. *Z. Ang. Math. Mech.,* **23,** 1–28.

Mass, C. F., and G. K. Ferber, 1990: Surface pressure perturbations produced by an isolated mesoscale topographic barrier. Part I: General characteristics and dynamics. *Mon. Wea. Rev.,* **118,** 2579–2595.

Miranda, P. M. A., and I. N. James, 1990: Surface pressure perturbations produced by an isolated mesoscale topographic barrier. Part II: Influence on regional circulation. *Mon. Wea. Rev.,* **118,** 2597–2606.

——, and ——, 1992: Non-linear three-dimensional effects on gravity wave drag: Splitting flow and breaking waves. *Quart. J. Roy. Meteor. Soc.,* **118,** 1057–1081.

Ólafsson, H., 1996: Morphologie et traînée de quelques écoulements orographiques de complexité croissante. Contribution à l'interprétation de PYREX. Thése de doctorat, Université Paul Sabatier, Toulouse, France, 312 pp.

——, and P. Bougeault, 1996: No linear flow past an elliptic mountain ridge. *J. Atmos. Sci.,* **53,** 2465–2489.

——, and ——, 1997: The effect of rotation and surface friction on orographic drag. *J. Atmos. Sci.,* **54,** 193–210.

Pettre, P., 1982: On the problem of violent valley winds. *J. Atmos. Sci.,* **39,** 542–554.

Phillips, D. S., 1984: Analytical surface pressure and drag for linear hydrostatic flow over three-dimensional elliptical mountains. *J. Atmos. Sci.,* **41,** 1073–1084.

Pierrehumbert, R. T., 1984: Linear results on the barrier effects of mesoscale mountains. *J. Atmos. Sci.,* **41,** 1356–1367.

——, and B. Wyman, 1985: Upstream effects of mesoscale mountains. *J. Atmos. Sci.,* **42,** 977–1003.
Queney, P., 1948: The problem of airflow over mountains: A summary of theoretical studies. *Bull. Amer. Meteor. Soc.,* **29,** 16–26.
Riosalido, R., L. Vasquez, A. Gordo, and A. Jansa, 1986: Cierzo: Northwesterly wind along Ebro valley as a mesoscale effect induced on the lee of the Pyrénées mountain range: A case study during ALPEX special observing period. GARP Publication Series 27, WMO/TD 108, 30 pp. [Available from WMO, Case Postale 2300, CH-1211, Geneva, Switzerland.]
Smith, R. B., 1978: A measurement of mountain drag. *J. Atmos. Sci.,* **35,** 1644–1654.
——, 1979a: Hydrostatic airflow over mountains. *Advances in Geophysics,* Vol. 31, Academic Press, 1–41.
——, 1979b: The influence of the heart's rotation on mountain wave drag. *J. Atmos. Sci.,* **36,** 177–180.
——, 1980: Linear theory of stratified flow past an isolated mountain. *Tellus,* **32,** 348–364.
——, 1982: Synoptic observations and theory of orographic disturbed wind and pressure. *J. Atmos. Sci.,* **39,** 60–70.
——, 1987: Aerial observations of the Yugoslavia bora. *J. Atmos. Sci.,* **44,** 269–297.
——, 1988: Linear theory of hydrostatic flow over an isolated mountain in isosteric coordinates. *J. Atmos. Sci.,* **45,** 3889–3896.
——, 1989: Mountain induced stagnation points in hydrostatic flow. *Tellus,* **41A,** 270–274.
——, and V. Grubisic, 1993: Aerial observations of Hawaii's wake. *J. Atmos. Sci.,* **50,** 3728–3750.
Smolarkiewicz, P. K., and R. Rotuno, 1989: Low Froude number flow past three-dimensional obstacles. Part I: Baroclinically generated lee vortices. *J. Atmos. Sci.,* **46,** 1154–1164.
Spangler, T. C., 1987: Comparison of actual dividing streamline heights to height prediction using Froude number. *J. Climate Appl. Meteor.,* **26,** 204–207.
Stein, J., 1992: Contribution à l'étude des régimes hydrostatiques d'écoulement orographiques. Ph.D. thesis, Université Paul Sabatier, Toulouse, France, 243 pp. [Available from CNRM, Meteo France, 31057 Toulouse, France.]
Thorsteinsson, S., 1988: Finite amplitude stratified airflow past isolated mountains on an f-plane. *Tellus,* **40A,** 220–236.
Vergeiner, I., 1971: Operational linear lee wave model for arbitrary basic flow and two-dimensional topography. *Quart. J. Roy. Meteor. Soc.,* **97,** 30–60.
Wurtele, M., 1957: The three dimensional lee wave. *Contrib. Atmos. Phys.,* **29,** 242–252.